Part III

Simulations Results: BTeV Physics Reach

Chapter 10

Status of the BTeV Simulation Effort

10.1 Update on MCFast

The physics simulations for BTeV have been carried out using MCFast v4_2 [1], a fast Monte Carlo package developed by the Fermilab Computing Division for detector design studies. MCFast provides a general framework for the comparison of differing detector geometries and is interfaced to a variety of generators that simulate the production and decay of B hadrons in a collider environment or fixed target environment.

The primary goal of MCFast is speed and flexibility which is achieved through parameterization. The package was designed to serve as an analysis tool that could be used to compare the physics reach of a variety of detector options. The program emphasizes fast tracing of particle trajectories through simple geometrical shapes. In the original version used for the EOI (MCFast v2_6), the particles were traced through the detector following a straight line or a helical trajectory. The effects of multiple scattering were added by calculating the track covariance matrix using a Kalman filter technique[2][3]. Smeared particle trajectories were supplied to the user for further analysis. Parameterized showering was implemented making it possible to simulate electromagnetic and hadronic showers and energy deposition inside calorimeters and absorbers. The simulation of showers in calorimeters and absorbers in MCFast is described in detail below. An interface between the MCFast geometry framework and GEANT was developed at this time and has been used for more detailed simulation of detector response.

In preparation for this document, we updated the package and have implemented multiple scattering, dE/dx, and bremsstrahlung during the tracing step. Decays in flight, pair conversions and secondary hadronic interactions are also included. Hits are now generated during the tracing step and are passed to a new track fitting package which is based on the Kalman filter technique. Realistic hit generation in the pixel detectors has been studied and a parameterized resolution as a function of track angle is included in the physics simulations presented here. The generated hits are also fed to the L1 trigger simulation package which does complete pattern recognition and has its own track fitter and vertex finder.

The current version of the MCFast package is written in Fortran and C and C^{++}. It is interfaced to the standard HEP event generators Pythia[6] , Herwig[7] and Isajet[8] through the StdHep interface. The decay of charm and bottom hadrons is done by QQ[9], a Monte Carlo package developed for CLEO. A 3-D Graphics package based on OpenInventor has been developed to display the detector geometry, tracks and hits.

MCFast v4_2 contains the new Kalman filter track fitter, and an optional C^{++} tracing and showering algorithm coupled to a more efficient hit generation package for the calorimeters. The new Kalman filter was used in the preparation of the results presented in this document and will be used extensively in future tracking studies. The C^{++} tracing and showering options, while complete, are still under test and were not used in the simulations presented in this document. The tracing and showering improvements will give us more efficient code and the ability to add radial detector elements such as a beampipes into the BTeV detector description.

Pythia 6.125 was used to generate physics processes for the BTeV simulation studies described below. Heavy quark decays were modeled through the CLEO decay Monte Carlo QQ 9.2b.

The size of the interaction region was taken as $\sigma_x = \sigma_y = 50\mu$m and $\sigma_z = 30$ cm corresponding to our current understanding of the running conditions in the C0 interaction region. The number of interactions per crossing is expected to be on average 2 at a luminosity of $2 \times 10^{32}\text{cm}^{-2}\text{s}^{-1}$ which means that there will often be more than one interaction per crossing. The effects of multiple interactions per crossing have been accounted for in these studies. The length of the interaction region and the station repetition in the vertex detector design allow us to separate tracks from two different primary interactions in each event as long as the interactions are more than a few centimeters apart.

10.2 Kalman Filter

In High Energy Physics today the method of choice for track fitting is Kalman Filtering [3, 5, 4], a method which produces an unbiased, optimal, linear estimator of the track parameters. By optimal it is meant that the estimator has the minimum variance of any unbiased, linear estimator. While these properties are only true in the limit of Gaussian multiple scattering, and Gaussian measurement errors, these conditions are sufficiently well approximated by the BTeV detector. The utility of the method is well established with operational experience in many HEP experiments. An important property of Kalman filtering is that it does not involve the inversion of large matrices and, therefore, that the execution time is linear in the number of hits. The method is also known in the HEP literature as Billoir fitting[2].

Since the last BTeV report, a Kalman Filter has been incorporated into MCFast for use a as stand-alone fitter. By stand-alone it is meant that the Kalman filter is not incorporated into the pattern recognition.

The present operation of MCFast is a two step process. In the first step, tracks are followed from their production point along their trajectory and, at each detector surface that is encountered, one or more operations takes place. These operations include multiple scattering, energy loss, elastic and inelastic hadronic scattering, bremsstrahlung and pair conversion. If the surface represents a sensitive element then a hit may also be created. In addition, decay in flight may occur at any point along the track and a shower may start when a particle passes through dense material such as magnet yokes, calorimeters and hadron filters. The collection of all points on one track which are recorded in this step is referred to as the trace list of the track. In the second step, the trace list of each track is used as the input to a Kalman filter. The output of the Kalman filter has been validated over the full range of momentum and angles which are important for BTeV.

With the advent of a working Kalman filter, several sorts of studies have become possible. These include the study of non-Gaussian resolution functions, validating the approximations used in the Level 1 trigger code, implementing the first Level 2 trigger algorithm and studying defects in pattern recognition.

The first of these has been carried out and is discussed in sections 10.3 and 5.2.2.4. The conclusion is that using realistic descriptions for the spatial resolution of the pixels grows only small non-Gaussian tails on all of the important physics quantities. All of these tails are small enough that they have no significant detrimental effect on the physics.

Because of stringent requirements on computing speed, the Level 1 trigger code must often make approximations for the properties of the tracks and vertices which it finds. For example, it may decide that the resolution on some quantity is sufficiently dominated by multiple scattering that other contributions to the resolution may be ignored. In order to verify these approximations the Kalman filter has been used to fit the tracks found by the Level 1 trigger. We have compared quantities computed by the trigger code to the corresponding quantities computed from the output of the Kalman filter; that is we are comparing the approximation against the best possible computation of the same quantity. This allows us to make quantitative judgments about the cost/benefit of replacing one approximation with another. This program has already resulted in improvements to the Level 1 trigger code and work is continuing.

A candidate Level 2 trigger algorithm, which is discussed in section 8.9, relies heavily on the Kalman filter code.

No results are yet available from the study of pattern recognition defects; they will be reported as they become available. The plan of this work is as follows. Before Kalman filtering a track we inspect the trace list and look for hits which do not belong to the track but which are close to it. If a hit is sufficiently close we add this hit to the trace list, either augmenting or replacing the nearby correct hit. This procedure grows tails in the physics distributions and, using this procedure, we will be able to estimate our sensitivity to errors in pattern recognition before a complete pattern recognition program is available.

Finally, the Kalman filter is already available for use as a final fitter once true pattern recognition algorithms are developed.

10.3 Towards Realistic Pixel Resolution Functions

The physics which governs the spatial resolution of the pixel detectors has been discussed in section 5.2.2. Using the results of that study, four different models of the spatial resolution of the pixel detectors have been incorporated into our simulations, the constant σ model, the variable σ model, fast clustering and slow clustering. The default model, the one used for most calculations presented in this document, is the variable σ model.

The constant σ model is the model used in the EOI. In this model the spatial resolution is a Gaussian with a constant width which is equal to the pitch divided by $\sqrt{12}$. This is true for both the short and the long measurement directions of the pixel.

In the variable σ model, the spatial resolution remains Gaussian but the width of the Gaussian for the short dimension of the pixel is a function of the angle of incidence of the track on the pixel plane. The width of the Gaussian for the long dimension of the pixel remains at the pitch divided by $\sqrt{12}$. For reference, the distribution of the x and y angles of incidence are shown in Fig. 10.1 parts a) and b). These figures were made using typical $b\bar{b}$ events and they only include hits from tracks with at least 20 hits. The width of the distribution for $\tan\theta_y$, is greater than that for $\tan\theta_x$ because of the bending of the tracks in the magnetic field of the analyzing dipole. Fig. 10.1 parts c) and d) show the value of σ, as a function of angle of incidence, for, respectively, pixels which measure x and pixels which measure y. The minimum of the y resolution is offset from $\theta_y =$ because of Lorentz force effects. These functions were made by making a piecewise linear approximation to the 2-bit data shown in Fig. 5.9, in section 5.2.2.4.

In the fast clustering model a Monte Carlo simulation is run for each intersection of a track with a pixel plane. Using the physics discussed in section 5.2.2, this simulation explicitly generates the digitized pulse heights recorded on nearby pixels. A 3-bit linear ADC and a threshold of 2000 e^- were assumed. Once each cluster has been generated, the pulse heights are used to obtain an estimator of the position of the hit; this estimator uses the knowledge of the angle of incidence.

In addition to returning an estimator of the (x, y) position of the hit, the fast clustering model also returns an estimate for the error on that position. This error is used by the Kalman filter and is similar to the error used in the variable σ model. Parts a) and b) of Fig. 10.2 show values of these errors for the short pixel dimension for hits on tracks, in typical $b\bar{b}$ events, with more than 20 hits. These functions are double valued because, at a given angle of incidence, not all tracks trigger the same number of pixels. A comparison with the corresponding plots for the variable σ model will show that, in significant parts of the cell, the resolution in the fast clustering model is slightly poorer. This, at first, seems surprising given that the fast clustering model uses more ADC bits. However, at the time that the fast clustering model was created, the Monte Carlo code which simulates the pulse heights had been improved by the addition of more processes which degrade the resolution. Fig. 10.2c) shows the quantity $(x_{\text{measured}} - x_{\text{generated}})/\sigma_x$ using the fast clustering model. In this figure there are two things to notice, one of which is the size of the non-gaussian tails; they are small enough to be manageable. The second is that the main part of the distribution is very box-like, which can be understood by seeing in part e) that, about half of the time, only a single pixel is hit. Because the resolution function of a single pixel is box-like, not Gaussian, the box-like shape makes an important contribution to part c). Parts d) and f) show similar information for pixels which measure y. In this case, however, the spreading due to the

Lorentz force ensures that, only rarely, is a single pixel hit; therefore the distribution in part d) is not box like. It also has quite small tails. The data in part d) which lie between -2 and 2 were fitted to a Gaussian and the width was measured to be 0.924 ± 0.005, which suggests that the fast clustering model returns values of σ_y which are usually a little too large.

The above discussion concerned only the resolution in the short dimension of the pixels. In the long dimension the nominal resolution is the pitch divided by $\sqrt{12}$ and, because almost all clusters are only one pixel wide, the shape of the resolution function is box-like.

The important improvement which is present in the fast clustering method is that its resolution functions are closer to reality, having a box-like component and noticeable tails. Using the fast clustering model, however, adds about 70% to the execution time of a typical physics analysis job. This is a sufficient degradation that this model is not routinely used for physics analyses and has only been used for a few specific studies. One such study, discussed in section 5.2.2.4, shows that the resolution functions discussed above do produce tails in several important physics quantities but that these tails are manageable.

The principal weakness of the fast clustering model is that the overlapping of two or more clusters is not considered. This weakness is addressed in the slow clustering model, in which the generation of pulse heights on pixels proceeds as in the fast clustering model. However the information about pulse heights on individual pixels is retained for a full event. Once an event has been fully generated, cluster finding code examines the wafers to identify clusters of hits and to estimate positions from the clusters. This code executes the most slowly of all models and has only been used for a few studies of occupancy. There are several obvious speed optimizations which can be applied to the implementation of this model and these optimizations are in the upgrade plan. The implementation of a fast algorithm which simulates overlapping clusters will be important for the simulation of the trigger.

A final improvement which is in the upgrade plan is to simulate clusters including delta ray production.

10.4 Multiple interactions per crossing

In BTeV, b events and c events represent, respectively, of order one part in 500 and one part in 100 of the total cross section. At design luminosity, $2 \times 10^{32}\mathrm{cm}^{-2}\mathrm{s}^{-1}$, we expect an average of 2 interactions per beam crossing. Therefore, to a good approximation, we can neglect the contribution of multiple b and c interactions in a single beam crossing. These considerations lead to the following simple model of multiple interactions which is implemented in MCFast.

MCFast requires the mean number of interactions per beam crossing and two input files, one containing signal events and the other containing background events. Typical background samples include events containing primary uds quarks, or generic QCD events, both as generated by Pythia. To generate one beam crossing, MCFast draws a number of interactions, n, from a Poisson distribution with the specified mean. If n is zero, then MCFast will redraw it. No record is kept of the frequency of redraws since that information is not needed to compute event yields. Once n is determined, MCFast will read one event from the signal file and $n-1$ events from the background file.

An upgrade is planned in which we deal with the fully general problem of many input streams, allowing zero or more interactions from all streams, as demanded by Poisson and multi-nomial statistics.

10.5 Simulation of Secondary Hadronic Interactions

Since the BTeV EOI, a new package has been added to MCFast to simulate secondary hadronic interactions. The approach is purely phenomenological, no attempt is made to model the underlying hard scattering process. The probability of an interaction occurring is determined by the collision length and absorption length of the material. Energy dependent cross-sections are not used.

10.5.1 Inelastic Secondary Interactions

The number of charged particles produced in a secondary interaction of a charged pion on a proton target is a function of s. The mean is given by

$$a + b\log s + c(\log s)^2.$$

where $a = -0.35$, $b = 1.21$ and $c = 0.03$ as given by Dumarchez et al. for pion-proton interactions [10]. The distribution is characterized by KNO scaling which is modeled as a truncated Gaussian. Fig 10.3 can be compared with Fig 5 in Firestone et al. [14]. For a heavier target the mean increases as a function of the atomic number A [11]. The average number of neutrals is assumed to be 50% of the charged multiplicity. The number of secondary particles from an interaction is limited to a maximum of 25 to avoid overflowing arrays.

The momentum distribution of secondary particles is approximately flat in rapidity and Gaussian in p_T with respect to the direction of the interacting particle [12]. The simulated distributions for a particle with momentum 50 GeV/c are shown in Fig 10.4. These can be compared with Fig 30 in Brenner et al.[12] and Fig 69 in [11]. The momentum of each outgoing particle is selected from these distributions and then energy is conserved by rescaling the momenta. The momenta are then rotated into the lab frame and the new particles are added to the StdHep list.

10.6 Elastic Interactions

Elastic scattering is characterized by the distribution of four-momentum transfer squared($-t = p_T^2$). The distribution is given by

$$d\sigma/dt = e^{(bt)}$$

where $b \approx 8$ [13]. The simulated distribution is shown in Fig 10.5.

10.7 Calorimeter Simulation

10.7.1 Simulation Techniques

We use three levels of simulation:

- Studies using the momentum vector of the generated photon, smeared according to simple resolution functions. This level of simulation can give insights into many issues and is fast (requires few computer resources). However, many details are beyond its scope. In particular, it does not distribute energy over calorimeter elements so one cannot use it to study or develop shower reconstruction. We have used it to study mass resolution in states containing photons and charged particles, to take a first look at combinatoric backgrounds, and to search for useful kinematic variables to cut on.

- Studies using a GEANT simulation. This is a full simulation of the shower development and involves tracking all the products of the cascade of pair conversions and bremsstrahlung. It contains detailed knowledge of all relevant physics processes. However, it takes a large amount of computer time and the generation of large numbers of events, especially for background rejection studies, is beyond our capabilities.

- Studies using the MCFast showering/calorimetry subpackage. This deposits (smeared) amounts of energy in detector elements based not on tracking of individual particles but based on parametrized shower shape distributions. This procedure does produce showers distributed over detector elements which can be processed by realistic shower reconstruction programs. The program executes much faster than a GEANT simulation but represents the energy deposition in detectors quite well and has been shown to be consistent with GEANT over the range of energies relevant to BTeV. We have used this program extensively in our background studies since the computer time is manageable.

All three methods have been used in designing the electromagnetic calorimeter and results obtained from each method appear in this document. Below we describe the MCFast program because it was used to produce the physics results presented in chapter 11.

10.7.2 The MCFast showering/calorimetry subpackage

The MCFast showering/calorimetry subpackage is completely integrated into the MCFast Monte-Carlo package: the user defines tracking systems and calorimeters and absorbers through the detector description file, and MCFast takes care of converting particles to showers automatically, through ad-hoc interruption of the tracing processes. In addition, energy losses and multiple scattering in the bulk material of the calorimeters and absorbers are taken into account.

As with other features of MCFast, the showering simulation is based on an extensive parametrization scheme. That is, there is no detailed, particle by particle, description of an electromagnetic or hadronic shower. Instead, the energy densities due to the high energy showering processes within volumes are parametrized, and shower fluctuations are simulated globably rather than locally. Then in calorimeters, these energy densities are mapped onto a user-controlled readout grid, and calorimetry hits are generated.

Unlike particle tracing in MCFast, the simulation of the shower propagation is intrinsically 3-dimensional. To keep the program simple, only three volume types are recognized: BOX, TUBE and CONE. These shapes must be oriented in such a way that the symmetry axis is along the Z-axis.

At the initialization stage, MCFast computes surface boundaries for these volumes. At the tracing stage, once such a surface is reached, the calorimetry subpackage returns an estimate of the mean free path length for the particle. For electrons/positrons and gammas it is simulated according the formula $f(x) = e^{-x/X_0}$, where X_0 is related to the radiation length. For hadrons $f(x) = e^{-x/\lambda}$, where λ is absorption length (the mean free path for inelastic interactions). Based on this information and a random number(s), the location of the interaction inside the calorimeter is computed, if need be. Should a primary interaction occur, the trace identity switches from "elementary particle" to "shower" and the core of that shower is propagated across the geometry by the MCFast tracing routine. This allows shower propagation from one calorimeter to the next.

Upstream of this conversion point, the particle behaves as a minimum ionizing particle (MIP), sensitive to magnetic field, if any, and undergoing energy loss and multiple scattering. The corresponding energy deposition is recorded, e.g., calorimetry hits are created.

Showering switches on at the shower conversion point. However, there is currently no provision for shower sensitivity to magnetic field inside a calorimeter. Unlike normal charged particles, the core of the shower propagates in a straight line.

Downstream of the conversion point, the deposited energy is calculated on a step by step basis, according to the shower longitudinal profile formulae. After each step, the shower core position and energy/momentum are estimated and the control is given to the hit generation if necessary. The package can optionally simulate energy deposition to the cells surrounding the shower core.

Note that a shower can spread over multiple volumes both longitudinally and transversely. Thus, even if a shower develops in an absorber, it still may produce hits in nearby calorimeters (if any).

The electromagnetic shower longitudinal profile is described as

$$dE/dx = E_0 b \frac{(bt)^{a-1} e^{-bt}}{\Gamma(a)}$$

where

$$t = x/X_0, \qquad b \simeq 0.5, \qquad a = 1 + bt_{max},$$

$$t_{max} = 1.0 \times (ln(y) + C_i), \qquad i = e, \gamma, \qquad (C_\gamma = +0.5, \qquad C_e = -0.5)$$

$$y = E/E_c, \qquad E_c = \frac{800MeV}{Z + 1.2},$$

(Z is atomic number, E_0 is energy of incident particle).

For hadronic showers we use

$$dE/dx = E_0(wb\frac{(bt)^{a-1}e^{-bt}}{\Gamma(a)} + (1-w)d\frac{(du)^{c-1}e^{-du}}{\Gamma(c)})$$

where

$$\begin{aligned} t &= x/X_0 \\ u &= x/\lambda \\ a &= 0.6165 + 0.3183 lnE_0 \\ b &= 0.2198 \\ c &= a \\ d &= 0.9099 - 0.0237 lnE_0 \\ w &= 0.4634 \end{aligned} \tag{10.1}$$

When the shower transverse profile is turned on, the energy deposited at each step is distributed around the shower axis according to the shower transverse profile (which becomes wider as the shower moves deeper into a calorimeter).

The transverse profile for both electromagnetic and hadronic showers is described as

$$\frac{dE}{dR} = e^{(-R/A_1)} + A_2 e^{(-R/A_3)}$$

In this formula, parameters A_1, A_2, A_3 depend on the material properties and on the current shower depth. The dependencies are different for electromagnetic and hadronic showers.

The distribution of deposited energy occurs in a plane perpendicular to the direction of motion of the shower core. Since showers may have crossed particular calorimeter boundaries, both longitudinally and transversely, energy deposition is also computed in the corresponding cells of those neighboring calorimeters.

The total deposited energy is smeared during the process of showering simulation according to the energy resolution formula

$$\frac{\sigma_E}{E} = \frac{a}{\sqrt{E}} \oplus b$$

where a and b are input parameters for the code. For a sampling calorimeter, a visible fraction of energy may be calculated (depending on the densities and proportion by volume of material from which a calorimeter is built).

In the version of MCFast (V4.2) used for the studies described below, energy deposition in calorimetric cells is organized in a list of “hits” in each calorimeter in the system, and the whole container of calorimetric hits in the system is organized as a “map”: the calorimeter

ID that refers to the geometry database vs. a list of hits in the calorimeter. A "Hit" refers to a set of variables describing the cell address, energy deposition via minimum ionization, electromagnetic, and hadronic processes, and information on particles/showers contributing to a given hit, i.e. track number referring to the HEP event list, along with the percentage of the hit total energy caused by the particle/shower.

As pointed out above, showers may spread over multiple volumes both longitudinally and transversely, and thus hits are produced in as many calorimeters as affected. And finally, calorimetric hits are available for analysis via a set of application user interface routines.

10.8 Simulation of the BTeV Trigger

Since the last BTeV report a great deal of work has gone into development of the trigger. This work includes improvements to the baseline Level 1 algorithm, an improved characterization and understanding of the baseline Level 1 algorithm, consideration of alternate Level 1 algorithms and a first look at details of a candidate Level 2 algorithm. Most of this work was done within the framework of the BTeV simulation package. The above material is discussed in chapter 8. Additional simulation of the queueing aspect of the Level 1 frontend has been done using the CNCL package [15]. Additionally, work on the DAQ system, which is intimately coupled to the details of the trigger implementation, is in progress. This material is discussed in chapter 9.

10.9 BTeV Geometry Description for MCFast

The geometry description for our MCFast simulations is more complete and more realistic than the one used in the EoI. The detector elements are better defined and the simulations reflect the more accurate estimates of material thickness and detector resolution. We have also taken into account multiple interactions and secondary interactions. Particles traced through the detector elements suffer the effects of multiple scattering, dE/dx and bremsstrahlung. Decays in flight and pair conversions are also included in the simulations. The trigger simulations use full pattern recognition in the tracking detectors. The physics simulation do not yet employ pattern recognition to build tracks from hits; the effects of the material thickness and realistic detector resolutions have been taken into account.

The standard geometry description of the baseline BTeV detector for MCFast physics studies includes:

- a dipole field described by 7 regions of constant field extending to ± 264 cm including the fringe and a yoke and coils which act as absorbers. The central 90 cm around the vertes detector is in a horizontal field of 1.6 T.

- a silicon pixel vertex detector with 31 stations with 3 planes each (Y-X-Y). The silicon and electronics is assumed to be 1 mm thickness and the outer layers of each have an extra 100 microns in thickness added to simulate the station shielding. The pixel dimensions are 50×400 micron. The resolution of the pixel detectors is parameterized as a function of angle.

- forward silicon detectors with 3 stations of strip detectors in each arm. Each station has 3 planes (i.e. 3 views X,Y,U). For these simulations, the strip pitch is 300 microns.
- a set of forward tracking chambers with 7 stations in each arm. The inner three devices in each arm have larger holes to accommodate the forward silicon tracker. There are 9 planes of straws with 3 views in each chamber (Y,U,V). The straw chamber resolution is assumed to be 150 microns.
- a RICH detector with C_4F_{10} gas and a Lucite mirror.
- an electromagnetic calorimeter with 2.47 cm $PbWO_4$ crystals which are 22.25 cm in length.
- muon system with muon detectors and absorbers. The muon detector and toroid simulations are described in Chapter 4, Section 4.2.7.

We have also generated a standard geometry description with a more detailed description of the vertex detector. Here each pixel chip is represented as an individual wafer and the wafers are in a tiled geometry. We have done studies of the trigger efficiency and resolution using this detailed description. The results of the resolution study are shown in Section 10.3.

The Level 1 vertex trigger algorithm including hit finding, pattern recognition, track finding and vertex finding is applied to each event during analysis in order to study the efficiency of vertex trigger. Level 2 trigger studies and muon trigger studies are currently underway and are described in detail in Chapters 8 and 4.

The physics simulations presented in this chapter use the standard baseline geometry description. The vertex detector is planned to be inside the beam pipe. The effects of the beam pipe on the outer tracker is currently under investigation.

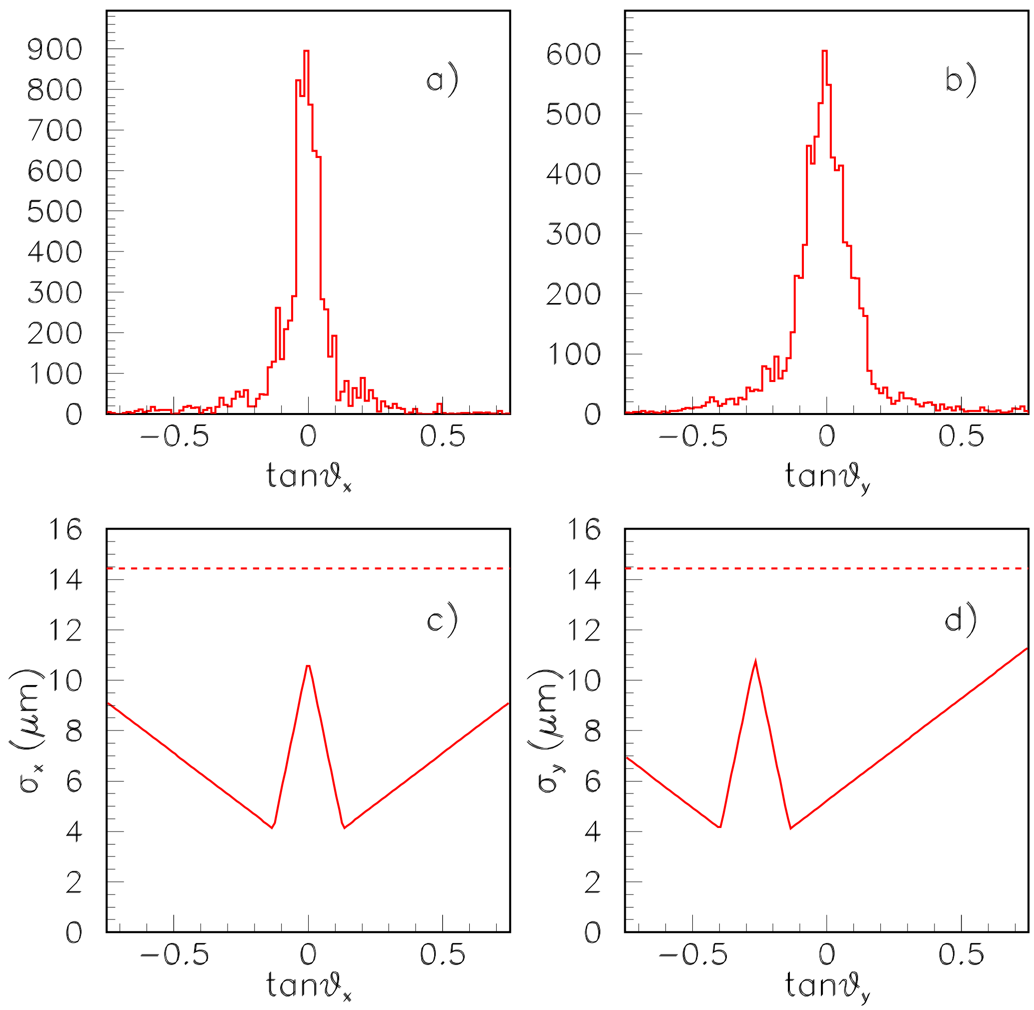

Figure 10.1: The distributions of a) $\tan\theta_x$ and b) $\tan\theta_y$ for hits on tracks, in $b\bar{b}$ events, with at least 20 hits. Here θ_x is the angle of incidence, in the xz plane, of a track which intersects a pixel detector. Similarly for θ_y. For most studies reported in this document, the pixel detectors are modeled as having a spatial resolution function which is Gaussian. The dependence of the σ of the Gaussian on angle of incidence is shown in c) for pixels which measure x and in d) for pixels which measure y. In both cases the solid line shows the value of σ for the short dimension while the dashed line shows the value for the long dimension.

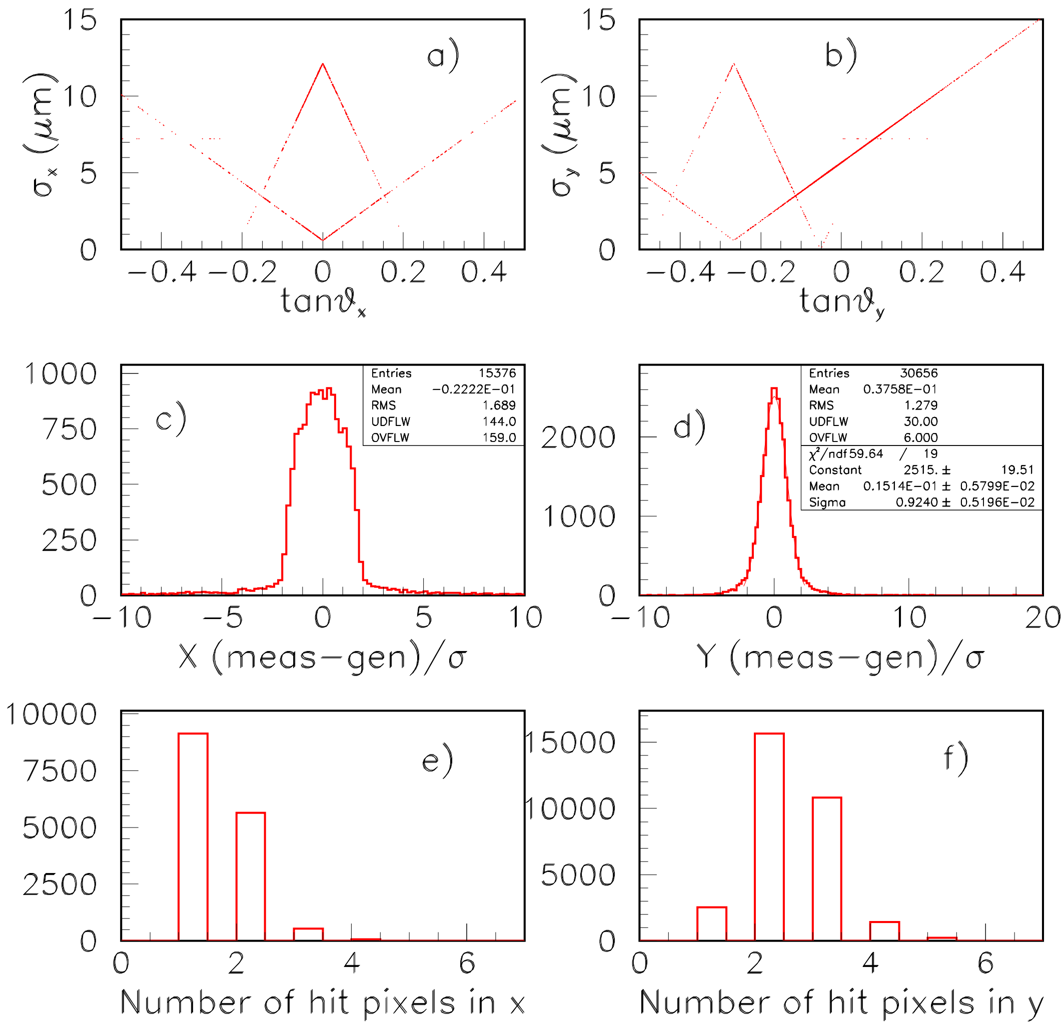

Figure 10.2: The values of the position errors in the fast clustering model for a) pixels measuring x and b) pixels measuring y. The angles θ_x and θ_y are defined in the caption of the previous figure. The functions are double valued because two tracks at the same angle of incidence may trigger a different number of pixels. The information in these figures is only for the short dimension of the pixel. Part c) shows the distribution of $(x_{\text{measured}} - x_{\text{generated}})/\sigma_x$ while part d) shows the corresponding distribution for y. The shapes of these distributions are discussed in the text. Parts e) and f) show the distributions of the number of pixels in a cluster.

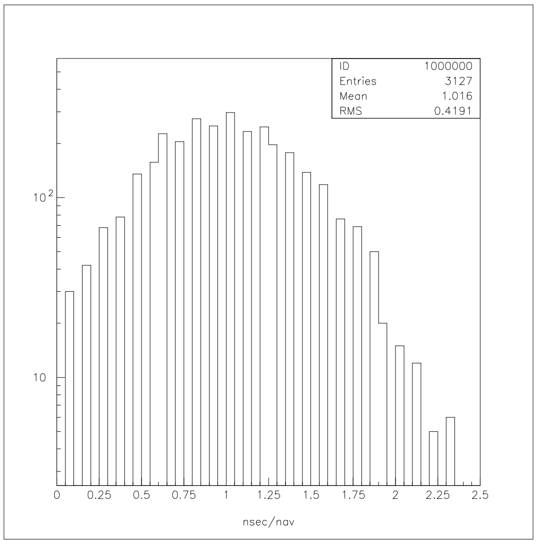

Figure 10.3: KNO scaling: $n_{sec}/ < n >$ is a universal distribution

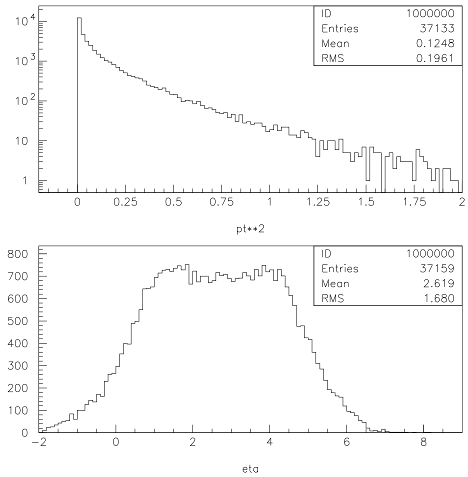

Figure 10.4: Simulated Kinematic distributions of secondary particles for an incident particle of 50 GeV/c (a) p_T, (b) η

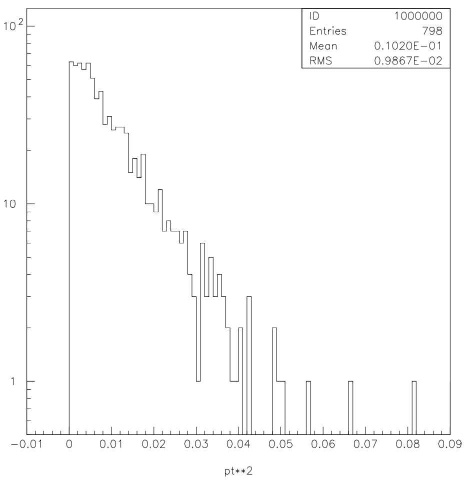

Figure 10.5: Simulated distribution of p_t^2 for elastic scattering

Bibliography

[1] P. Avery et al, "MCFast: A Fast Simulation Package for Detector Design Studies". in the Proceedings of the International Conference on Computing in High Energy Physics, Berlin, (1997) and http://fnpspa.fnal.gov/mcfast/mcfast_docs.html

[2] P. Billoir, NIM **225**, 352-366 (1984).

[3] Paul Avery http://www.phys.ufl.edu/˜avery/fitting.html, Fitting Theory V.

[4] R. Bock et. al., "Data Analysis Techniques for High-Energy Physics Experiments", Cambridge University Press (1990).

[5] M.Regler and R. Fruwirth, "Reconstruction of Charged Particle Trajectories", Plenum Publishing Company (1989).

[6] H. U. Bengtsson and T. Sjostrand, Comput. Phys. Comun. **46**,43 (1987).

[7] G. Marchesini and B.R. Webber, Nucl. Phys. **B310**, 461 (1988); Nucl. Phys. **B330**, 261 (1988);
I. G. Knowles, Nucl. Phys. **B310**, 571 (1988);
G. Abbiendi, *et al.*, Comp. Phys. Comm. **67**, 465 (1992).

[8] F. Paige and S. Protopopescu, Brookhaven National Laboratory Report BNL-37066(1985)(unpublished).

[9] QQ is developed and maintained by the CLEO Collaboration. See http://www.lns.cornell.edu/public/CLEO/soft/QQ/ For the studies reported here, it is used for its model of the decays of hadrons containing heavy flavors.

[10] "Average Multiplicity and KNO Scaling in Hadron-Hadron Interactions", J. Dumarchez et al, Il Nuovo Cimento **66A**, 114 (1981)

[11] " GHEISHA: The simulation of Hadronic Showers - Physics and Applications", H. Fesefeldt, PITHA 85/02

[12] "Experimental Study of single-particle inclusive hadron scattering and associated multiplicities", A. Brenner et al, Phys. Rev. D **26** 1497(1982)

[13] "Hadron-proton elastic scattering at 50, 100, and 200 GeV/c momentum", C. W. Akerlof et al, Phys. Rev. D **14** 2864 (1976)

[14] "$\pi^- p$ interactions at 360 GeV/c: Measurement of the total and elastic cross sections and the charged-particle multiplicity distribution", A. Firestone et al., Phys. Rev. D **14** 2902 (1976)

[15] See http://www.comnets.rwth-aachen.de/doc/cncl.html.

Chapter 11

The Physics reach of BTeV

In this chapter, we present results of physics simulations of some of the key measurements discussed in chapters 1 and 2. We begin with three techniques for measuring the CKM angle γ. We also discuss two channels useful for getting information on the CKM angle α, $B^o \to \rho\pi$ and $B^o \to \pi^+\pi^-$. We also present one result on a typical rare decay, $B^+ \to K^+\mu^+\mu^-$ and one involving a photon, $B^o \to K^{*o}\gamma$. We include a discussion of the measurement of $B^o \to \psi K_s$ and present our sensitivity for the measurement of B_s mixing. We also present studies on several methods of flavor tagging.

In calculating the number of events per year that we expect to reconstruct we assume a luminosity of $\mathcal{L} = 2 \times 10^{32}\text{cm}^{-2}\text{s}^{-1}$. In this work MCfast was used to determine the "reconstruction efficiency". MCfast provides the user with a list of smeared tracks that are within the geometrical acceptance, each characterized by a list of hits for each subdetector. Cuts on these hit multiplicites are typically applied on each of the tracks and other topological cuts may be applied. The reconstruction efficiency is based on these cuts and does not reflect possible losses due to pattern recognition defects.

11.1 Measurement of the CKM angle γ

There have been several suggestions on how to measure the CKM angle γ (see chapter 1, section 9). There are discrete ambiguities inherent in all of these methods so using several methods will help remove some of these ambiguities as well help control systematic errors. We give a status report here of our simulations of three methods.

11.1.1 $B_s \to D_s K$

This method measures the CP violation resulting from the interference of direct and mixing induced decays.

When a final state f can come from both a pure B^0 and a pure $\overline{B}^0$, the amplitudes for the direct decay $B^0 \to f$ and the mixing induced sequence $B \to \overline{B}^0 \to f$ can interfere. A time dependent CP-violating effect can thus appear. Consider the following decay widths [1]:

$$\Gamma_1 = \Gamma(B \to f) = |M|^2 e^{-t}\{\cos^2(xt/2) + \rho^2 \sin^2(xt/2) - \rho \sin(\phi + \delta)\sin(xt)\}$$

$$\Gamma_2 = \Gamma(\overline{B} \to \overline{f}) = |M|^2 e^{-t}\{\cos^2(xt/2) + \rho^2 \sin^2(xt/2) + \rho \sin(\phi - \delta)\sin(xt)\}$$

$$\Gamma_3 = \Gamma(B \to \overline{f}) = |M|^2 e^{-t}\{\rho^2\cos^2(xt/2) + \sin^2(xt/2) - \rho \sin(\phi - \delta)\sin(xt)\}$$

$$\Gamma_4 = \Gamma(\overline{B} \to f) = |M|^2 e^{-t}\{\rho^2\cos^2(xt/2) + \sin^2(xt/2) + \rho \sin(\phi + \delta)\sin(xt)\},$$

where $M = \langle\, f|B\rangle$, $M' = \langle\, f|\overline{B}\rangle$, $\rho = |M'/M|$, $x = \Delta m/\Gamma$, δ is the strong phase difference between the two decays $B \to f$ and $B \to \overline{f}$, and ϕ is the relative CKM phase of the two decay amplitudes.

The time-dependent CP asymmetry is given by:

$$\begin{aligned} A_{CP}(t) &= \frac{[N(B\to f) + N(B \to \overline{f})] - [N(\overline{B} \to f) + N(\overline{B} \to \overline{f})]}{[N(B\to f) + N(B \to \overline{f})] + [N(\overline{B} \to f) + N(\overline{B} \to \overline{f})]} \\ &= \frac{\Gamma_1 + \Gamma_3 - \Gamma_2 - \Gamma_4}{\Gamma_1 + \Gamma_3 + \Gamma_2 + \Gamma_4} \\ &= \frac{2\rho}{\rho^2+1}\cos(\delta)\sin(\phi)\sin(xt)\ . \end{aligned}$$

The CP asymmetry is optimized if $2\rho/(\rho^2+1) \approx 1$, ie. the branching fractions of the decays into f and $\overline{f}$ are of the same order of magnitude.

A particularly useful case is where the B_s decays into the final states $f \equiv D_s^+ K^-$ and $\overline{f} \equiv D_s^- K^+$. The branching fractions are expected to both be $\sim 10^{-4}$ and in this case the weak angle $\phi = \gamma$. Note that the final state is almost identical to the more prolific mode $D_s^+\pi^-$. Clearly, the particle identification is crucial here.

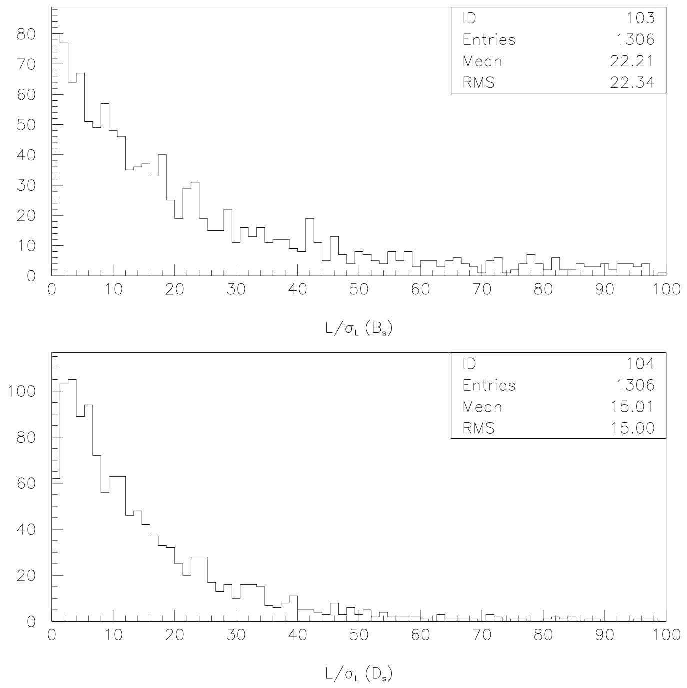

Figure 11.1: (top) $L/\sigma_L(B_s)$, (bottom) $L/\sigma_L(D_s)$

From a time-dependent measurement of the 4 decay rates $B_s \to D_s^+ K^-$, $B_s \to D_s^- K^+$, $\overline{B}_s \to D_s^- K^+$ and $\overline{B}_s \to D_s^+ K^-$ one can extract the quantities $\sin(\gamma + \delta)$, $\sin(\gamma - \delta)$ and ρ, assuming that the value of x_s will have been determined in a separate measurement. The quantity $\sin\gamma$ then can be extracted up to a 2-fold ambiguity.

The main handle we have at triggering on and reconstructing these decays is the detachment of the secondary B_s and tertiary D_s decay vertices. The distributions of detachment length divided by the resolution in the detachment L/σ_L are shown in Fig 11.1. We require $L/\sigma_L(D_s) > 4.0$ and $L/\sigma_L(B_s) > 4.0$.

We have studied the reconstruction and trigger efficiencies of $B_s \to D_s K$ using both the $\phi\pi$ and K^*K decay modes of the D_s. The combined geometric acceptance and reconstruction efficiency of these modes is 2.0% for the $\phi\pi$ mode and 1.7% for the K^*K, with a signal to background of about 10:1. The signal is shown in Fig. 11.2. The Level 1 trigger efficiency is 70% after all other cuts have been applied. Using branching ratios given by Aleksan et al. [31] and a tagging efficiency $\epsilon = 40\%$ we expect a total of 2680 tagged events (sum of 4 decay modes) in 10^7 sec.

The CP asymmetry is diluted by time smearing, mistagging and background. The proper time resolution must be small to resolve the B_s oscillations. Fig. 11.3 is a plot of the generated proper time minus the reconstructed proper time for events passing the cuts described above. The proper time is calculated from the decay length where the decay point of the B_s comes

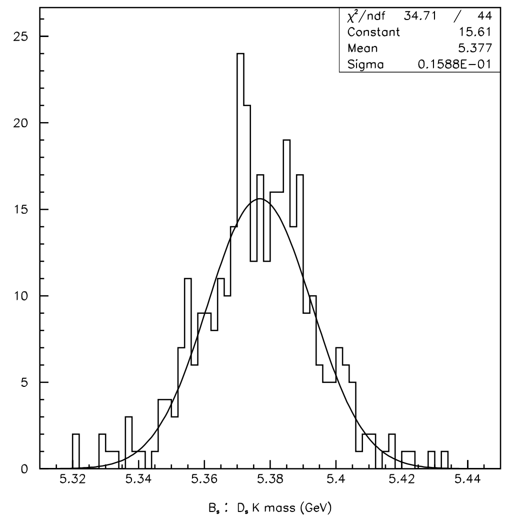

Figure 11.2: Mass Resolution for B_s

from the vertex fit of the D_s with the K. A Gaussian fit to the $t_{gen} - t_{res}$ distribution gives $\sigma_t = 0.045$. Given that $\tau_{B_s} = 1.54$ psec, then $\sigma_t/t = 0.030$.

We estimated the accuracy in determining γ as follows. First, a set of "events" (*ie.* proper times) was generated, split into the 4 decay modes with correct time distributions. The values of the parameters were chosen to be $x_s = 20.0$, $\rho = 0.5$, $\gamma = 45^o$ and $\delta = 23^o$). Theoretically, the strong phase δ is expected to be small [2]. The proper times were smeared with a Gaussian of width $\sigma_t = 0.030\tau$. and a cut-off at low t simulated an L/σ_L cut: $t_{min} = 0.25\tau$. A fraction of the events were then assigned to come from the "wrong flavor" parent. A mistag fraction of 30% is used. This includes mistagging due to mixing of the other B. Background events with a pure exponential time distribution are added to the "signal" events. The background is assumed to have the same lifetime as the signal.

In the absence of dilution factors the probability function is of the form:

$$P_1(t) = e^{-t}\{\cos^2(xt/2) + \rho^2 \sin^2(xt/2) - \rho \sin(\gamma+\delta)\sin(xt)\}$$

In the presence of dilution factors the following changes are made to the probability function:

(a) to correct for time smearing:

$$\begin{aligned} P_1^{'}(t) &= \int_{-\infty}^{\infty} dt^{'} \frac{e^{-(t-t^{'})^2/2\sigma^2}}{\sqrt{2\pi\sigma^2}} P_1(t) \\ &= e^{\sigma^2/2}e^{-t}[\cos^2(x(t-\sigma^2))(1+e^{-x^2\sigma^2/2}+\rho^2(1-e^{-x^2\sigma^2/2}))+ \\ &\quad \sin^2(x(t-\sigma^2))(1-e^{-x^2\sigma^2/2}+\rho^2(1+e^{-x^2\sigma^2/2}))+\sin(x(t-\sigma^2))\sin(\gamma+\delta)], \end{aligned}$$

(b) to correct for background:

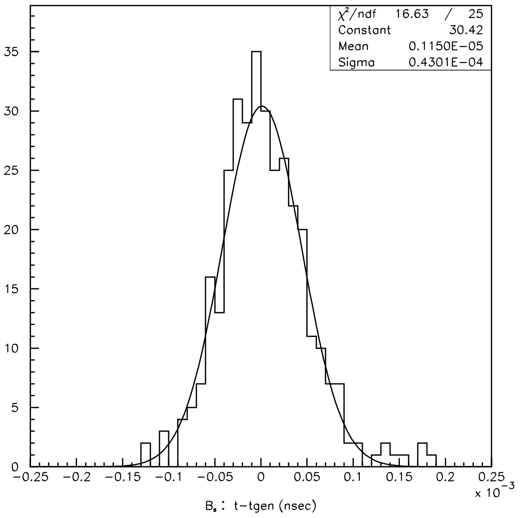

Figure 11.3: Proper Time Resolution for B_s : $t_{gen} - t_{rec}$ (nsec)

$$P_1^{''}(t) = P_1^{'}(t) + e^{-t}B, \tag{11.1}$$

(c) to correct for mistagging:

$$P_1^{'''}(t) = (1-w)P_1^{''}(t) + wP_4^{''}(t), \tag{11.2}$$

The value of $\sin\gamma$ can be extracted from $\sin(\gamma+\delta)$ and $\sin(\gamma-\delta)$ with a 4-fold ambiguity which reduces to a 2-fold ambiguity if it is assumed that $\sin\gamma > 0$. This still leads to a 4-fold ambiguity in the value of γ. If the true value of $\sin(\gamma+\delta)$ or $\sin(\gamma-\delta)$ is close to 1.0 then the fitted values may be outside the physically allowed region. In particular, this is likely when the number of events is small and hence the errors are large.

In order to study the obtainable accuracy on γ we ran 1000 "experiments," each with a signal of 2680 events where we fitted $\sin(\gamma+\delta)$ and $\sin(\gamma-\delta)$ and then calculated $\sin\gamma$ and $\cos\delta$, setting $\sin(\gamma+\delta)$ and $\sin(\gamma-\delta)$ to be equal to 1.0 if the fitted value was greater than 1.0. The results are shown in Fig. 11.4.

If $x_s = 20$ and $\rho = 0.5$ then it will be possible to measure $\sin(\gamma+\delta)$ and $\sin(\gamma-\delta)$ with a statistical error of ± 0.15 in one year of running at $\mathcal{L} = 2\times 10^{32}\mathrm{cm}^{-2}\mathrm{s}^{-1}$. This will give an error on γ of about 11^o. The largest potential experimental problem with this method occurs when x_s is near 60. Then the time smearing dominates the error and the measurement error increases substantially.

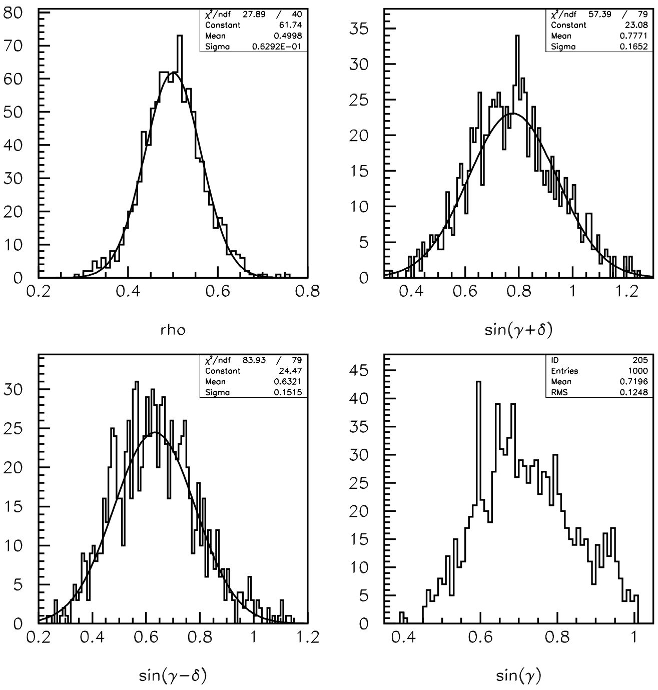

Figure 11.4: Fitted values of ρ, $\sin(\gamma+\delta)$, $\sin(\gamma-\delta)$, and $\sin\gamma$. Input parameters $\rho = 0.5$, $\sin(\gamma+\delta) = 0.771$, $\sin(\gamma-\delta) = 0.629$, $\sin\gamma = 0.703 (\gamma = 45^o)$. Results of fit: $\gamma = 46^{+11^o}_{-9^o}$

11.1.2 $B^- \to K^- D^0$

Another method for extracting γ has been proposed by Atwood, Dunietz and Soni [3], who refined a suggestion by Gronau and Wyler [4]. In the decay $B^- \to K^- D^0$ a CP asymmetry can result from the interference of the decays $B^- \to K^- D^0, D^0 \to f$ and $B^- \to K^- \overline{D}^0, \overline{D}^0 \to f$. In particular if f is a doubly Cabibbo suppressed decay of the D^0 then this asymmetry may be large. The weak phase difference between $B^- \to K^- D^0$ and $B^- \to K^- \overline{D}^0$ is γ. To observe a CP asymmetry there must also be a non-zero strong phase between the two amplitudes. It is necessary to measure the branching ratio $\mathcal{B}(B^- \to K^- f_i)$ for at least 2 different states f in order to determine γ up to discrete ambiguities. This method measures direct CP violation and requires neither tagging nor time-dependent measurements.

Define the following quantities :

$$a = Br(B^- \to K^- D^0) \tag{11.3}$$

$$b = Br(B^- \to K^- \overline{D}^0) \tag{11.4}$$

$$c(f1) = Br(D^0 \to f1), \quad c(f2) = Br(D^0 \to f2) \tag{11.5}$$

$$c(\overline{f1}) = Br(D^0 \to \overline{f1}), \quad c(\overline{f2}) = Br(D^0 \to \overline{f2}) \tag{11.6}$$

$$d(f1) = Br(B^- \to K^- f1), \quad d(f2) = Br(B^- \to K^- f2) \tag{11.7}$$

$$\overline{d}(f1) = Br(B^+ \to K^+ f1), \quad \overline{d}(f2) = Br(B^+ \to K^+ f2) \tag{11.8}$$

It is assumed that we will measure the quantities a, $c(f1)$, $c(f2)$, $c(\overline{f1})$, $c(\overline{f2})$ $d(f1)$, $d(f2)$, $\overline{d}(f1)$ and $\overline{d}(f2)$ but not b.

We can express $d(f1)$ in terms of a, b, $c(f1)$, $c(\overline{f1})$, the strong phase ξ_1 and the weak phase γ.

$$d(f1) = a * c(f1) + b * c(\overline{f1}) + 2\sqrt{a * b * c(f1) * c(\overline{f1})}\cos(\xi_1 + \gamma) \tag{11.9}$$

$$\overline{d}(f1) = a * c(f1) + b * c(\overline{f1}) + 2\sqrt{a * b * c(f1) * c(\overline{f1})}\cos(\xi_1 - \gamma) \tag{11.10}$$

$$d(f2) = a * c(f2) + b * c(\overline{f2}) + 2\sqrt{a * b * c(f2) * c(\overline{f2})}\cos(\xi_2 + \gamma) \tag{11.11}$$

$$\overline{d}(f2) = a * c(f2) + b * c(\overline{f2}) + 2\sqrt{a * b * c(f2) * c(\overline{f2})}\cos(\xi_2 - \gamma) \tag{11.12}$$

These four equations contain the 4 unknowns ξ_1, ξ_2, b, γ which can be determined up to discrete ambiguities.

We have studied the reconstruction and trigger efficiencies of decay modes $B^- \to K^-[K^+\pi^-]$ and $B^- \to K^-[K^+K^-]$. The combined geometric acceptance and reconstruction efficiency was found to be 3.8% for the $K\pi$ mode and 2.5% for KK. We expect that the RICH will provide excellent particle ID, so we believe that most of the background in the $B^- \to K^-[K^+\pi^-]$ mode will come from events where a real D^0 decays via the Cabibbo favored mode and combines with a kaon from the other B. We have studied this type of background and expect to achieve S/B$\sim$1.

The trigger efficiency is approximately 60% for both modes. The expected number of $B^\pm$ events in 10^7 s is 320 in the $K\pi$ mode and 1600 in the K^+K^- mode (see Table 11.1). The reconstructed signal is shown in Fig. 11.5.

In order to estimate our ability to measure γ, several sets of input parameters (b, γ, ξ_1, xi_2) were chosen and for each set the expected number of events in each channel was calculated . Then 1000 trials were done for each set, smearing the number of events by $\sqrt{N+B}$. The results of one set of trials showing the distribution in fitted values of b and γ are shown in Fig. 11.6.

With this number of events we expect to be able to measure γ (up to discrete ambiguities) with a statistical error of about 13^o in one year of running at $\mathcal{L} = 2 \times 10^{32}\mathrm{cm}^{-2}\mathrm{s}^{-1}$. The overall sensitivity depends on the actual values of γ and the strong phases.

Table 11.1: Expected Number of ($B^- \to K^- D^0$) Events

	$B^- \to K^-(K^+\pi^-)$	$B^- \to K^-(K^+K^-)$
(a)= BR($B^- \to K^- D^0$)	2.5×10^{-4}	
(b)= BR($B^- \to K^- \overline{D^0}$)	2.2×10^{-6}	
($\overline{c1}$)= BR($D^0 \to K^-\pi^+$)	.04	
(c1)= BR($D^0 \to K^+\pi^-$)	3.1×10^{-4}	
(c2)= BR($D^0 \to K^+K^-$)		4.3×10^{-3}
$(a) \times (c1) + (b) \times (\overline{c1})$	1.7×10^{-7}	
$(a) \times (c2)$		1.1×10^{-6}
Reconstruction efficiency	0.038	0.025
Trigger efficiency	0.60	0.60
N events/year $B^{\pm}$	320	1600

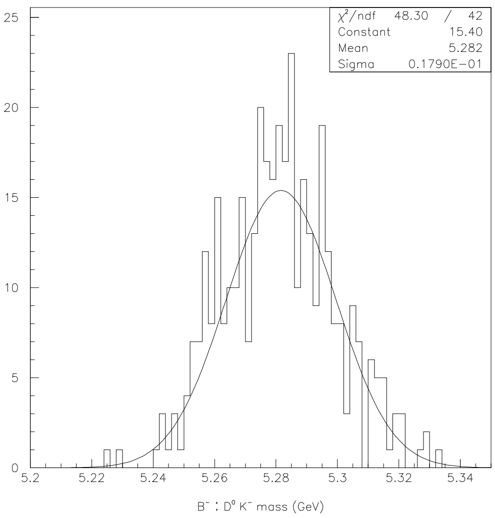

Figure 11.5: $D^0 K^-$ mass

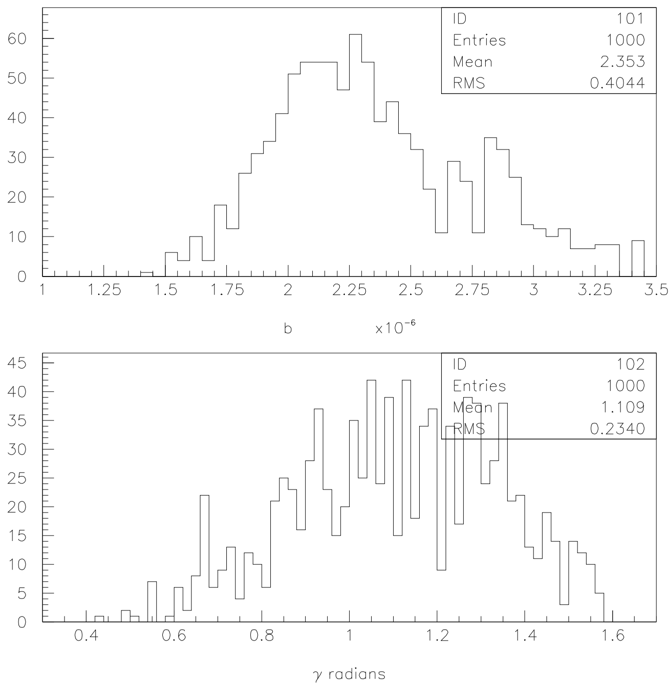

Figure 11.6: Calculated values of γ and b for 1000 trials with input parameters $\gamma = 65^o$, (1.13 rad), $b = 2.2 \times 10^{-6}$

11.1.3 $B \to K\pi$

This method uses the branching ratios of the decays $B^+ \to \pi^+ K^0$ and $B^0 \to \pi^- K^+$ and their complex conjugates as explained in a paper by Gronau and Rosner [5]. The decay $B^+ \to \pi^+ K^0$ proceeds only through a penguin amplitude and the decay $B^0 \to \pi^- K^+$ proceeds through both penguin and tree amplitudes. Ignoring electroweak penguin contributions, the penguin amplitudes in the charged and neutral B decays to $K\pi$ are equal.

It is useful to define

$$R \equiv \frac{\Gamma(B^0 \to K^+\pi^-) + \Gamma(\overline{B}^0 \to K^-\pi^+)}{\Gamma(B^+ \to K^0\pi^+) + \Gamma(B^- \to \overline{K}^0\pi^-)}$$

$$A^{'} \equiv \frac{\Gamma(B^0 \to K^+\pi^-) - \Gamma(\overline{B}^0 \to K^-\pi^+)}{\Gamma(B^+ \to K^0\pi^+) + \Gamma(B^- \to \overline{K}^0\pi^-)}.$$

An expression for γ can be given in terms of R, $A^{'}$ and the ratio of tree to penguin amplitudes $r \equiv |T|/|P|$.

If we define δ to be the phase difference between the penguin and tree amplitudes, the ratios R and $A^{'}$ can be rewritten :

$$R = 1 - 2r\cos\gamma\cos\delta + R^2$$

$$A^{'} = 2r\sin\delta\sin\gamma$$

Combining these equations to eliminate δ we get

$$R = 1 + r^2 \pm \sqrt{4r^2\cos^2\gamma - A'^2\cot^2\gamma}$$

Fleischer and Mannel[6] have claimed that if $R < 1$ a useful bound can be obtained regardless of the value of r or δ:

$$\sin^2\gamma \leq R$$

If we have information on r we can get a more precise estimate of γ.

CLEO has determined $R = 0.65 \pm 0.40$, which suggests that the ratio could be less than 1.0 [7]. If this result holds with improved statistics then this method compliments other methods in that it will begin to exclude some of the region around $\gamma = \pi/2$.

There has been much discussion about the effect of final state interactions on the measured branching ratios. Falk et al. [8] have shown that contributions to $B^+ \to \pi^+ K^0$ from rescattering of channels such as $B^+ \to \pi^0 K^+$ lead to a modification of the Fleischer-Mannel bound:

$$\sin^2\gamma \leq R(1 + 2\epsilon\sqrt{1-R})$$

where ϵ is the ratio of the rescattered amplitude to the penguin amplitude. They estimate $\epsilon = O(0.1)$. This rescattering contribution can be determined by measuring the K^+K^- final state branching ratio, which BTeV is well equipped to do.

To study the reconstruction efficiency of $B^+ \to \pi^+ K_s$ Monte Carlo events were generated using PYTHIA with the decays of charm and bottom particles being handled by QQ. First the primary vertex was found then K_s candidates were selected by combining all pairs of oppositely charged tracks not identified as kaons. These tracks were required to have an impact parameter greater than 5σ with respect to the primary vertex, to form a vertex with $\chi^2 < 5$ and to be within 6 MeV of the nominal K_s mass. The K_s vertex was required to have $l/\sigma > 6$ with respect to the primary vertex. B candidates were selected by combining the K_s candidates with all other charged tracks not identified as kaons and having an impact parameter greater than 3.5σ with respect to the primary vertex. The reconstructed B candidate was required to have $l/\sigma > 4$, and point back to the primary with an impact parameter less than 2.5σ. The combined geometric acceptance and reconstruction efficiency of the $B^+ \to \pi^+ K_s$ mode is 2.8% and the trigger efficiency is 40%. The reconstructed signal is shown in Fig. 11.7.

The background has been studied using 500K generic $b\overline{b}$ events with minimum bias events added to give an average of two interactions per beam crossing. Only one event with a mass above 5 GeV/c^2 survived the cuts as described above. From these limited statistics we estimate we can achieve a signal to background ratio of about 1:1 .

The decay mode $B^0 \to \pi^- K^+$ has also been simulated. The two prong vertex should easily be distinguished from background with an l/σ cut and the requirement that the reconstructed B point back to the primary vertex. The reconstruction efficiency is found to be 9.8% and the trigger efficiency for events which pass the analysis cuts is 54%. The signal is shown if Fig 11.8. The background has not yet been studied but the signal to background ratio is expected to be better than that for $B^0 \to \pi^+\pi^-$ $(S/B = 0.6)$ because $B^0 \to \pi^- K^+$ has a higher branching ratio and there are fewer kaons than pions so the combinatoric background is lower.

We expect to reconstruct 11,000 $B^\pm$ and 110,000 $B^0/\overline{B}^0$ in 10^7 s of running at $\mathcal{L} = 2 \times 10^{32}\mathrm{cm}^{-2}\mathrm{s}^{-1}$. Gronau and Rosner [5] have estimated that a 5° precision in γ can be achieved with 2400 events in each channel. This of course, doesn't take into account the above mentioned theoretical criticisms of the technique.

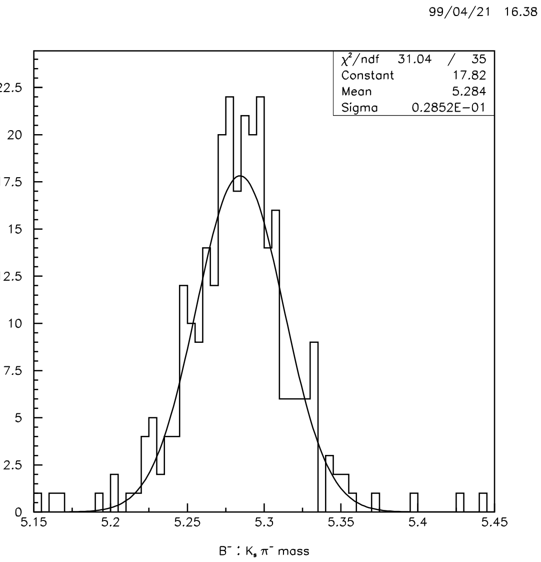

Figure 11.7: $K_s\pi$ mass

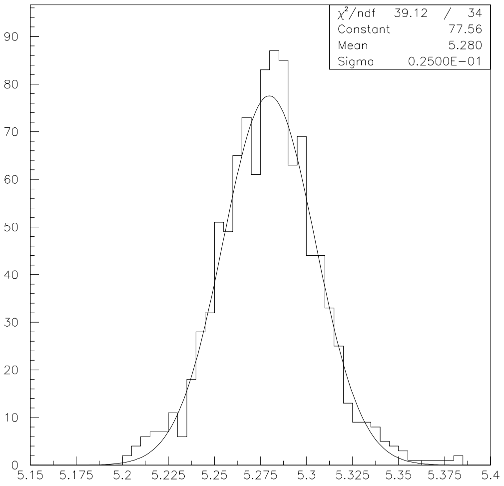

Figure 11.8: $K^+\pi^-$ mass

11.2 $B_d^0 \to J/\psi K_s$

The decay $B_d^0 \to J/\psi K_s$ is the golden mode for measuring the CP violating angle β. A study has been made of the reconstruction efficiency and trigger efficiency of the proposed BTEV/C0 detector for the decay $B_d^0 \to J/\psi K_s \to \mu^+\mu^-\pi^+\pi^-$

The dominant backgrounds to the decay channel $B^0 \to \psi K_s$ are expected to arise from J/ψ's from B-decays combining with real K_s's from fragmentation or J/ψ's coming directly from hadronization combining with any K_s. CDF found that prompt J/ψ's are a large fraction of total J/ψ production [10] and that this fraction increases as p_t decreases. In the forward geometry of the BTEV/C0 detector the p_t of the J/ψ's accepted peaks at about 2 GeV/c (see Fig 11.9). Extrapolating from the CDF results we expect that J/ψ's from B decays only comprise about 5% of the total J/ψ production. Background from fake or prompt J/ψ's can be reduced by a cut on the distance between the primary vertex and decay vertex. Monte Carlo events of the type $B \to J/\psi X$ were generated to study the background arising from J/ψ's from B-decays.

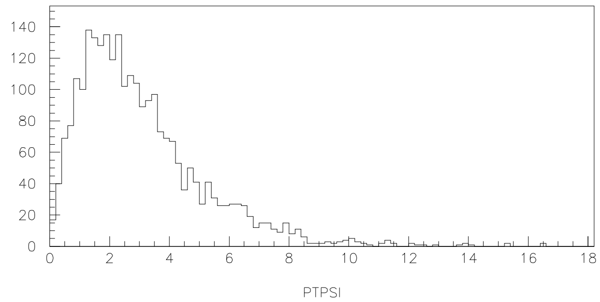

Figure 11.9: p_t distribution of J/ψ's

To study the reconstruction efficiency Monte Carlo events were generated using PYTHIA with the decays of charm and bottom particles being handled by QQ. The following requirements were put on all events:

- Each event must pass a primary vertex fit.
- J/ψ candidates were selected by combining pairs of oppositely charged tracks identified as muons. The muons were required to have a momentum greater than 5.0 GeV, and have a least one hit in the muon detector. These tracks were then required to pass a vertex fit. The normalized distance between the primary vertex and J/ψ vertex (l/σ) was required to be greater than 4.0. This cut is 80% efficient for the signal and rejects 99.95% of the background from prompt J/ψ's. (see Fig 11.10)
- K_s candidates were selected by combining pairs of oppositely charged tracks with a minimum momentum of 0.5 GeV and fitting them to a vertex. Each track was required

to miss the primary vertex by at least 3σ and the reconstructed K_s was required to point back to the J/ψ vertex to within 3σ. (Figs 11.11 and 11.12).

- The J/ψ and K_s candidates within a 3σ mass window of the nominal values were combined to form B_d^0 candidates. To reduce the background from K_s's from the primary vertex combining with a J/ψ from a B decay we require the K_s impact parameter to the secondary vertex divided by the impact parameter to the primary vertex to be less than 2.0. We also require that the reconstructed B^0 point back to the primary vertex.

The reconstructed signal and background are shown in Fig 11.13. The reconstruction efficiency of the signal is 4.0%. This signal is from 10K generated events.

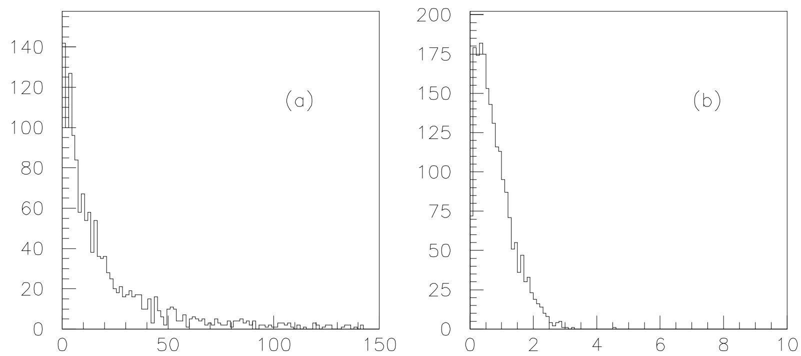

Figure 11.10: L/σ (a)J/ψ from B decays, (b) J/ψ from primary vertex

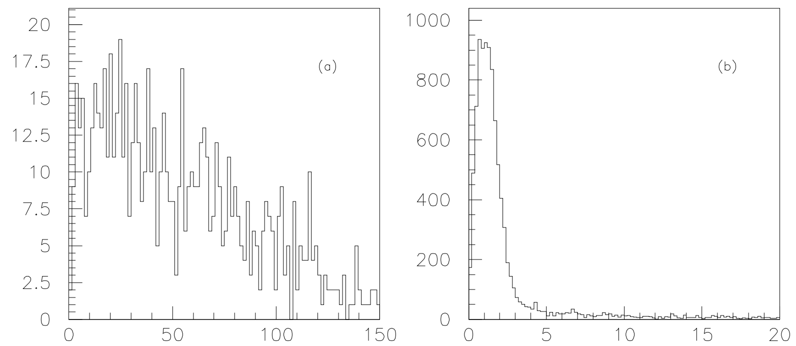

Figure 11.11: Normalized Impact parameter with respect to the primary vertex of (a) π's from real K_s's , (b) π's from fake K_s

The number of signal and background events expected in 10^7 sec of running time is shown in Table 11.2. We estimate that the efficiency of a dimuon trigger with a threshold of 10 GeV/c is 70% for events which pass the analysis cuts. The efficiency of the Level 1 vertex

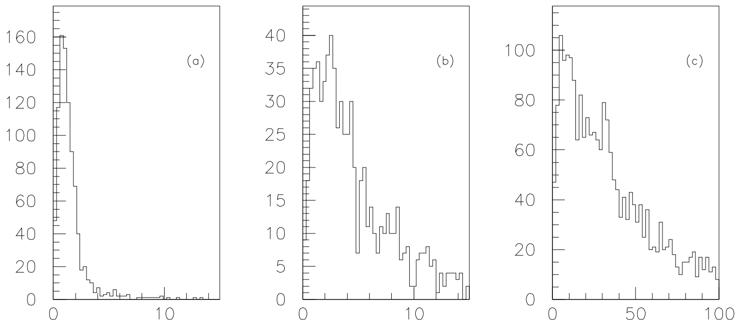

Figure 11.12: Normalized Impact parameter with respect to J/ψ vertex (a) real K_s from $B \to J/\psi K_s$ decay, (b) other real K_s's, (c) Fake K_s's

trigger is approximately 50% for these events so we estimate a total trigger efficiency of 85%. For a time integrated asymmetry measurement the error on sin2β is given by

$$\delta\sin(2\beta) = \frac{1+x_d^2}{x_d}\frac{1}{\sqrt{\epsilon D^2 N}}\sqrt{\frac{S+B}{S}}$$

where $x_d/(1+x_d^2) = 0.47$ accounts for the dilution due to the time evolution of the B_d^0. We estimate the effective tagging efficiency ϵD^2 to be 10% (see section 11.3) and assume $S/B = 10$ which results in a value of $\delta\sin(2\beta)$ of 0.021. A time dependent analysis of the asymmetry will result in a more accurate determination of $\sin(2\beta)$.

Table 11.2:

Luminosity	2×10^{32}
Running time	10^7 sec
$\sigma_{b\bar{b}}$	100μb
Number of $B\overline{B}$ events	2×10^{11}
Number of $B_d^0/\overline{B_d^0}$'s	1.6×10^{11}
$\mathcal{B}(B_d^0 \to J/\psi K_s^0)$	5×10^{-4}
$\mathcal{B}(J/\psi \to \mu^+\mu^-)\times\mathrm{B}(K_s^0 \to \pi^+\pi^-)$	0.04
Reconstruction efficiency	0.04
Trigger efficiency	0.85
Number of reconstructed $B_d^0 \to J/\psi K_s^0$	109,000
Tagging efficiency ϵD^2	10%
$\delta\sin(2\beta)$	0.021

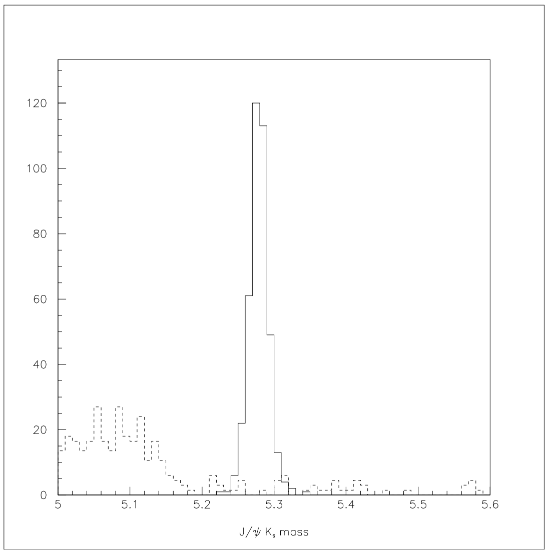

Figure 11.13: $J/\psi K_s$ mass - solid line: signal, dashed line: background from B decays to $J/\psi X$. Most of the background below 5.15 GeV/c^2 is from $B \to J/\psi K^*$ decays

11.3 Flavor Tagging

For charged B mesons, the flavor of the heavy quark (b or $\bar{b}$) is determined by the charge of the B mesons. For neutral B mesons (B_d and B_s) the quark flavor can usually be determined from the flavor of the decay products, for example by the charge of the kaon in $B_s \to \psi \bar{K}^*$, $\bar{K}^* \to K^-\pi^+$ decay. These modes can be used to measure $B_s \leftrightarrow \bar{B}_s$ and $B_d \leftrightarrow \bar{B}_d$ oscillations (sensitive to V_{ts} and V_{td} respectively), if the flavor of the b quark at the production point is determined independently. Decays to CP-eigenstates do not identify the b quark flavor. In fact, amplitudes for these decays interfere with the mixing amplitude producing CP-violating effects. Measurements of CP-asymmetry, resulting e.g. in determination of $\sin 2\beta$ via $B_d \to \psi K^0_S$, again require determination of the b quark flavor at the production point - so called "flavor tagging". Since every tagging method sometimes produces false identification, the effectiveness of flavor tagging is characterized by an effective tagging efficiency ϵD^2 where $\epsilon = (N_R + N_W)/N$, and D is a "dilution" factor, $D = (N_R - N_W)/(N_R + N_W)$, where $N-$number of reconstructed signal events, N_R-number of right flavor tags in this sample, N_W-number of wrong flavor tags. Since the measurements mentioned above are among the most important goals of the BTeV program, large tagging efficiency is a crucial design criterion for the experiment. The forward detector geometry offers unique advantages for flavor tagging over an experiment operating in the central region.

The *Away Side Tagging* methods rely on determination of the flavor of the other b quark in the event, since b quarks are always produced in $b\bar{b}$ pairs. The flavor of the other b can be determined from the charge of the lepton emitted in its semileptonic decay, the overall charge of the b jet, or the charge of the kaon produced in the $b \to c \to s$ cascade.

A study had been made of the efficiency of Jet Charge tagging in the BTeV detector. PYTHIA was used to generate $b\bar{b}$ events where the $\bar{b}$ was fragmented into a B^0 which was then forced to decay via the decay chain $B^0 \to J/\psi K_s, J/\psi \to \mu^+\mu^-, K_s \to \pi^+\pi^-$. No restrictions were placed on the b fragmentation and QQ was modified to include incoherent mixing of neutral B mesons [12].

An "opposite jet" is a combination of tracks consistent with being decay products of the other B. Candidate tracks for the opposite jet must have a transverse momentum greater than 100 MeV/c and are required to miss the primary vertex by more than 3σ. Due to the fact that the B's are produced close in pseudorapidity we require that the difference in pseudorapidity between the opposite jet candidates and the B^0 be less than 4.0 units or that both B's be in the same arm of the detector. The opposite jet is identified as a combination of tracks with a common secondary vertex which is separated from the primary by at least 1.0σ. If more than one jet is found, the one with the highest transverse momentum is selected, and if there is no secondary vertex passes the cuts as described then the highest p_t track is selected, provided that the p_t >1.0 GeV/c.

The jet charge is calculated according to the formula:

$$Q_{jet} = \frac{\sum_i q_i \cdot (\vec{p}_i \cdot \hat{a})^k}{\sum_i (\vec{p}_i \cdot \hat{a})^k}$$

where q_i and p_i are the charge and momentum of the i^{th} track, $\hat{a}$ is the jet axis and k is a weighting factor that we choose to be zero. When the b hadronizes into a $\overline{B}$, the opposite jet typically has a neutral charge and useful tagging information is not obtained. However this has the advantage that this method is not affected by mixing. The results of this study indicate that we can achieve a tagging efficiency $\epsilon = 0.39$ and a dilution $D = 0.41$ which results in an effective efficiency $\epsilon D^2 = 0.065$.

Lepton tagging is limited by the low branching ratio for semi-leptonic decays and wrong-sign background that results from semileptonic charm decays in $b \to c$ cascades. A study of muon tagging has been made using the same $B \to J/\psi$ events as the Jet Charge tagging study. The muons from the decays of B and D mesons have quite different p_t distributions so some separation can be achieved by this method. Our simulations indicate that we can achieve $\epsilon\, D^2 \approx 0.016$ for muon tagging.

Kaon tagging is the most potent method at e^+e^- B factories. Potentially large backgrounds from the underlying event call for excellence in both particle identification and vertex resolution. Both are strong points of our forward detector geometry. As described in the detector design section we are aiming at efficient kaon identification in the 3-70 GeV/c momentum range. Even with a perfect kaon identification there is a large kaon background from the underlying event which may dilute tagging efficiency. Figure 11.14 illustrates the importance of a good resolution on the kaon impact parameter at the primary vertex for suppression of this background. In BTeV the tagging efficiency is improved by a large factor when cutting on significance of the impact parameter of the kaon. This figures also illustrates that the impact parameter resolution achievable in a central detector is not sufficient for a large improvement in tagging based on kaon identification. In BTeV, we expect kaon tagging efficiency $\epsilon\, D^2$ in a range of 4.5-6% depending on the exact performance of the particle identification system.

The *Same Side Tagging* method uses the correlations which arise between the B meson and the charge of nearby tracks produced in the fragmentation chain or from B^{**} decays. For B_s mesons the correlation is with a charged kaon. Preliminary studies indicate that this method is particularly useful for B_s tagging where we expect to achieve $\epsilon D^2 > 5.0\%$.

We have not yet studied the correlations between different tagging methods but estimate we can achieve an overall effective tagging efficiency ϵD^2 of about 10%.

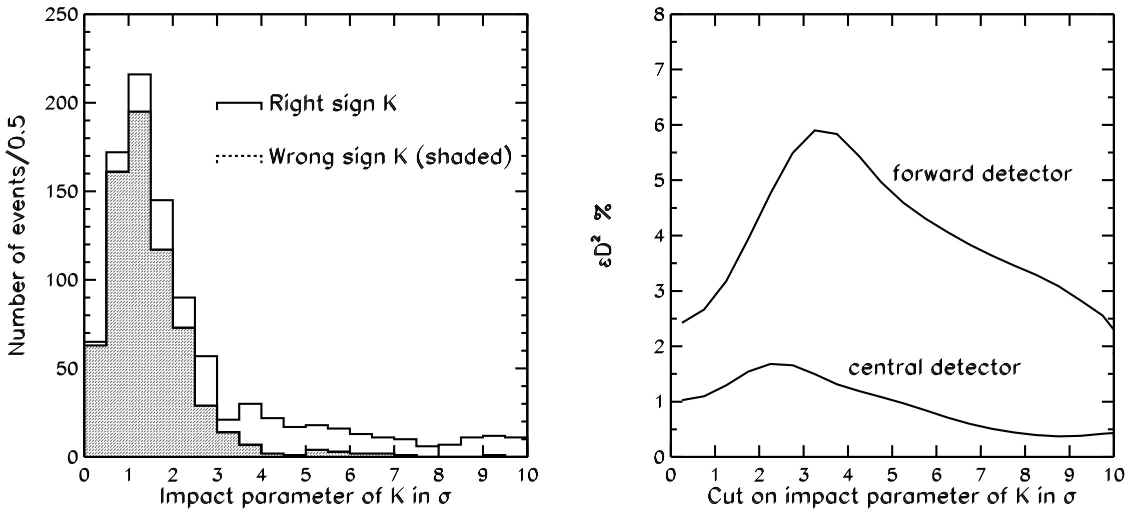

Figure 11.14: *Left plot:* L/σ distribution in BTeV for K impact parameter for right sign (unshaded) and wrong sign (shaded) tags. *Right plot:* Kaon tagging efficiency ($\epsilon\, D^2$) as a function of kaon impact parameter cut in units of L/σ. Particle misidentification is neglected. The upper curve represents BTeV simulation. The lower curve represents a central detector with a ToF system and vertex detector with SVX-II performance.

11.4 $B_d \to \pi^+\pi^-$

The decay $B_d \to \pi^+\pi^-$ is the traditional choice for measuring $\sin(2\alpha)$, but the evidence for large penguin amplitudes in the observation of $B_d \to K^+\pi^-$ by the CLEO collaboration means that a simple extraction of $\sin(2\alpha)$ from this mode is no longer likely. However, this mode has been used to benchmark so many experiments it is still worthwhile to understand. In addition, it may be useful for the extraction of γ when combined with a measurement of $B_s \to K^+K^-$ as explained in section 1.9.4.

The signature for this decay is very simple: two oppositely charged tracks with a displaced vertex and the invariant mass of a B^0. Most of the background rejection against random combinations must come from the secondary vertex. While particle identification is vital to reject backgrounds from decays like $B^0 \to K^+\pi^-$ and $B_s \to K^+K^-$, it has a small effect on random combinations since most particles are pions.

It has been shown by the BCD group [13] that the dominant background to $B^0 \to \pi^+\pi^-$ comes from random combinations of tracks in events containing B's. Tracks from real B's are already displaced from the primary vertex and have a higher probability of faking a secondary vertex. We have chosen to optimize our selection to minimize the background from real B decays. Further studies will be needed to confirm that this is also sufficient to reject charm and light quark backgrounds.

We generated all our events samples using PYTHIA and QQ to decay the charm and bottom particles. One signal interaction and n background interactions were used where n was selected to simulate a poisson ditribution of mean 2.0. This is equivalent to a luminosity of 2×10^{32} cm^{-2} s^{-1}.

For this analysis we fit the primary vertex from tracks that are known to come from the primary. This underestimates the error on the primary but not significantly and the error on the decay distance is still dominated by the secondary decay. We loop over *all* opposite sign tracks with nine or more hits in the silicon vertex detector and try to fit a secondary vertex. Those with $\chi^2 < 2.0$ are kept for further analysis. After these fits we need to make four selections to reduce the random backgrounds:

- the cosine of the opening angle of the $\pi^+\pi^-$ pair must be greater than zero. Random tracks that are in opposite hemispheres of the detector produce masses near the B, while real B's in our acceptance never have opening angles this large.

- require that the distance between the primary and secondary decay divided by its error, L/σ, be greater than 15. This cut strongly rejects random combinations where tracks come from the primary vertex.

- require that each pion miss the primary vertex by more than 5 times its error on the impact parameter with respect to the primary vertex. This is correlated with the previous cut, but it can reject situations where a primary vertex track crosses another track making a false secondary vertex.

- require that the B^0 point back to the primary vertex within 2σ of its point back error. This requirement rejects false vertices that consist of two tracks from different secondary decays.

Pattern recognition in the silicon sets the requirement that each of the two π track candidates have hits in 9 planes (3 stations) of the vertex detector. The geometric acceptance for $B^0 \to \pi^+\pi^-$ where both tracks are required to hit 3 stations is about 23%. The reconstruction of the primary and secondary vertices and the background rejection cuts have an efficiency of 8.4% which means that over one third of the events in the acceptance remain after the cuts are applied.

There are several decay modes of B mesons that can mimic a $B_d \to \pi^+\pi^-$ decay. The decay $B_s \to K^+K^-$, which is due to a hadronic penguin decay mechanism, is the most important with other contributions from $B_d \to K^+\pi^-$ and $B_s \to K^-\pi^+$. Recent results from CLEO show a confirmed signal for the $B_d \to K^+\pi^-$ decay and an upper limit on the decay of interest, $B_d \to \pi^+\pi^-$[7]. While many people have previously made assumptions that the $\pi\pi$ mode was larger than or equal to the $K\pi$ mode, it now appears that the $K\pi$ mode is larger. Based on the CLEO yields of each we will make a conservative assumption that $\mathcal{B}(B_d \to K^+\pi^-)$ is twice a large as $\mathcal{B}(B_d \to \pi^+\pi^-)$.

$B_s \to \pi^+K^-$ is a $b \to u$ transition of the B_s similar to the decay $B_d \to \pi^+\pi^-$, and $B_s \to K^+K^-$ is a hadronic penguin. The modes of B_s decays are normalized by having the total B_s production be 34% of B_d production [14]. In addition, we expect that the penguin and $b \to u$ decays of the B_s will have the same pattern of branching ratios as the B_d.

Using the above results as input, we simulate the two pion mass plot without particle identification in Fig. 11.15. The plots make it clear that kinematic separation is inadequate to discriminate between these decays. The width and separations for the signals in the mass plot are almost identical to CDF's prediction in their TDR [16], although they used a more favorable ratio of $K\pi$ to $\pi\pi$ which the new CLEO data puts in doubt.

MCFast does not simulate the RICH response, but it can model the geometric acceptance, momentum threshold, decays in flight and secondary interactions. The efficiency after accounting for these effects is 6.5%. Misidentification in the RICH at the 1-2% level will produce a background that is quite small compared to the background due to random combinations and it can be ignored.

There is a strong correlation between triggered events and reconstructed events. For a trigger requirement of two tracks with more than 4σ significant miss distance from the primary vertex, the simulation shows that more than 50% of our reconstructable events pass this trigger. Such a trigger requirement rejects the light quark background at a rate of 100 to 1. This leaves us with 34,000 events per year of running before flavor tagging of the opposite b has been attempted.

Our signal to background estimate is based on 280,000 generic B events, which were selected at the generator level to have two tracks with a mass within 500 MeV/c^2 (about 18 times our mass resolution) of the B^0 mass. The two tracks also had to have an opening angle less than $\pi/2$. These cuts reduce the sample that we need to examine by a factor of 13, so our effective background sample is 3,700,000 events.

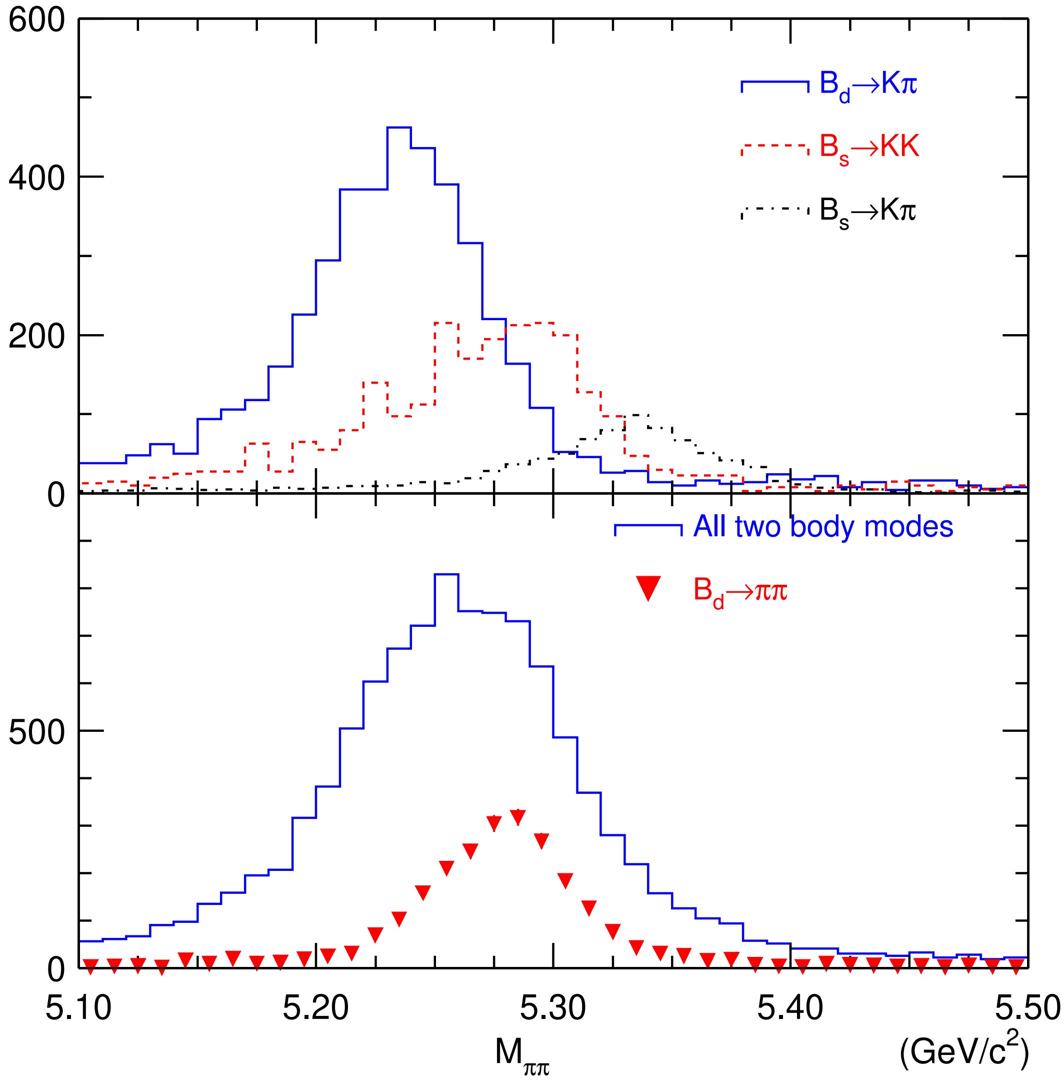

Figure 11.15: Two body mass plots without particle identification a) $B_d \to K^+\pi^-$, $B_s \to \pi^+K^-$, $B_s \to K^+K^-$, b) $B_d \to \pi^+\pi^-$ and a sum of all two body decay modes. All particles are assumed to be pions.

Table 11.3: Projected yield of $B^0 \to \pi^+\pi^-$ and the uncertainty on a_{CP}

Luminosity	$2 \times 10^{32}\mathrm{cm}^{-2}\mathrm{s}^{-1}$
Running time	10^7 sec
Integrated Luminosity	2000 pb^{-1}
$\sigma_{b\bar{b}}$	100 μb
Number of $B\overline{B}$ events	2×10^{11}
Number of B_d^0's	1.4×10^{11}
$\mathcal{B}(B_d^0 \to \pi^+\pi^-)$	0.75×10^{-5}
Reconstruction efficiency	0.06
Trigger efficiency	0.50
Number of reconstructed $B_d^0 \to \pi^+\pi^-$	3.4×10^4
Tagging efficiency ϵD^2	0.10
S/B	0.6
δa_{CP}	0.023

From this sample only 1 event has a $\pi\pi$ mass that lies between 5.1 and 5.5 GeV, and if we scale to a B signal region which is 150 MeV wide ($\sigma = 25$MeV) we expect less than one event under the peak. We will assume that the background has 1 event due to the limited statistics. If we assume a branching ratio $\mathcal{B}(B_d \to \pi^+\pi^-) = 0.75 \times 10^{-5}$, then our $S/B = 0.6$ but with large errors. Study of larger samples of backgrounds may allow us to understand how to improve our signal to background ratio.

The tagging efficiency, which is discussed in Section 11.3, is estimated to be 10%. We can combine these results to find an uncertainty on the CP asymmetry. Our results are shown in Table 11.3.

11.5 $B^o \to K^{*o}\gamma$

The decay $B^o \to K^{*o}\gamma$ is an example of a relatively rare decay involving a single photon. This decay has already been observed by CLEO, with branching fraction $(4\pm1.7\pm0.8)\times10^{-5}$. Decays such as $B^o \to K^{*o}\gamma$, $B^o \to \rho^o\gamma$, $B_s \to \phi^o\gamma$, and $B_s \to K^{*o}\gamma$ provide insight into $\frac{V_{td}}{V_{ts}}$. We have chosen to study $B^o \to K^{*o}\gamma$ because its branching fraction is measured so a definite predictions of the reconstructed event yield is possible. Here the K^{*o} decays into $K^+\pi^-$. This state can benefit from the kinematic cuts and the p_t requirements described below to suppress the combinatoric background. Decays such as $B^o \to \rho^o\gamma$ are expected to have much smaller branching fractions and backgrounds which are comparable so more work will have to done on background rejection to prove that their detection is possible.

In order to calculate the effective signal, one has to design analysis cuts that suppress the backgrounds. A major source of background is from $B^{o,\pm} \to K^{*o}\ +\ X$ in combination with a photon from either the underlying event or the other B. Since the expected signal is so small compared to potential sources of background, a very large number of events must be simulated to demonstrate that the signal will not be overwhelmed. The simulation of an adequate number of events requires more computing resources than we have so we have had to make some assumptions. Within the context of these assumptions, we have obtained a fairly good estimate of the background to our signal.

The basic assumptions that we have made in estimating the background are:

- Non-B events can be adequately suppressed by selecting events that have a well-defined primary vertex and a downstream decay vertex;
- The B events that will cause backgrounds to this process will contain a $K^{*o}(890)$ (we do not require this to come from downstream of the primary vertex in our initial selection); and
- The events that satisfy the above requirements will only create background if they contain at least one photon which makes a high invariant mass– greater than 4.0 GeV/c^2 – when combined with the K^{*o}.

With these assumptions, we can reject 98% of all generic $B-\bar{B}$ events at the 'event generator' level. We only have to perform the full detector simulation, reconstruction, and analysis on the surviving 2%. We have used 400,000 events which survived from 20,000,000 at the event generator level to compute the background. Even this large number of events is still marginal for the background estimation since each background event surviving the analysis and appearing in the $K^{*o}\gamma$ mass plot represents 10,000 events per year.

In the analysis presented below, we have assumed a calorimeter resolution with a stochastic term of 2.5% and a constant term of 0.55%. If, as expected we can do better than this, the mass resolution will improve.

11.5.1 An Initial Shower Reconstruction Program

The use of the showers generated by MCFast (or GEANT) in a realistic analysis requires a shower reconstruction program. Such a program looks for $PbWO_4$ blocks with locally high maxima of energy deposition and uses them to 'seed' showers. Nearby blocks are then aggregated around the seed blocks to form the complete showers. The number of blocks to include around the seed is usually determined by GEANT simulations or from beam tests. Various techniques are used to partition energy (on a statistical basis) between showers which share cells.

We do not yet have a shower reconstruction program so we are using a 'prompted' reconstruction program. In this program, we trace the generated photons to the calorimeter to get the seed block. After that, we compute the shower energy as the sum of the energies of the seed block, the nearest neighbor blocks, and the next-to nearest neighbor blocks. A total of twenty-five blocks are summed which is consistent with our GEANT studies. The position is computed from the energy-weighted first moment of the blocks in X and separately in Y. The correction to the position described in chapter 4 is not applied yet. π^o's are reconstructed simply by looping over all showers, computing the invariant mass of each pair, and cutting on the mass. No asymmetry cuts or other cuts intended to improve signal to background are made at this point.

Features of the current approach which cause it to depart from reality are:

- The current program does not permit one to find 'false' showers because it starts from the generated photons. This may result in underestimation of the combinatoric background. In a complete analysis, charged hadrons and electrons can be rejected by observing tracks pointing near the shower centroid so they in general are not a source of false photon candidates. bremsstrahlung photons, neutral hadrons, and artifacts of the reconstruction program can, however, create extraneous neutral showers.

- Since all photons, electrons, and hadrons deposit energy in the calorimeter, realistic problems with overlapping showers exist. The simple algorithms we are using do not guard against such overlaps so that some showers will have their energy and/or position distorted. This causes the efficiency of shower reconstruction to be lower than what we ultimately expect to achieve.

This simple approach will be replaced as soon as possible by a full reconstruction program which will remedy all of these defects. However, the techniques we have used to reject combinatoric backgrounds, described in the next section, should work very well to suppress the additional backgrounds from the extraneous showers described above so we expect that the background will not be too much worse than what we see now. Moreover, there are real opportunities for improved efficiencies with an improved reconstruction program.

11.5.2 Suppression of Combinatoric Backgrounds

Before the advent of precision vertex detectors, the study of heavy quark states produced in hadronic interactions and decaying into all charged particles was nearly impossible due to combinatoric backgrounds. That is, mass combinations with the same particle content as the signal, but coming from the non-heavy quark events or the underlying part of a genuine heavy quark event, populated the mass region of interest with many more entries than did the real signal. The mass peak was then lost or obscured in the fluctuations of this background. Silicon vertex detectors permitted one to cluster the charged tracks into vertices and to include in signals only the tracks that came from a well-defined decay vertex observed downstream of the main interaction. This effectively eliminated the combinatoric background in many heavy quark decays and made possible successful programs of heavy quark studies in photoproduction and hadroproduction.

For final states containing both charged particles and neutral objects such as photons and π^os, one must again face the threat of being overwhelmed by combinatoric backgrounds. The vertex detector can be used to reconstruct the primary vertex and the B vertex from the charged particles and to isolate a reasonably pure sample of B events. Then the charged tracks in these vertices can be combined with photons or π^o candidates to form the final state of interest. The problem is that the calorimeter must be at the downstream end of the system far from the interaction vertex and we know of no technology that will determine the position and direction of the neutral objects striking it well enough to tell whether they come from the primary vertex, the secondary vertex of interest, or other secondary vertices in the event. It seems then that we have to form mass combinations of every photon or π^o candidate with the charged tracks and that this could produce large combinatoric backgrounds that would obscure or highly pollute any signals.

There are two ways to combat combinatoric background by eliminating many of the photons or π^os from consideration as objects in the B decay of interest. The first is by taking advantage of some kinematic features of the photons from the decays of interest which differentiate them from other photons. The second is by exploiting the fact that in BTeV we have a rather good knowledge of the direction of the B and we can insist that only photons or π^o's that balance the transverse momentum of the charged tracks relative to the B direction be considered as daughters of the B decay.

Kinematic cuts are effective when the photons from the B final state under study have very different properties from other photons in the event. This is true, for example, for quasi-two-body decays onto a single photon and a hadronic resonance. Prime examples are

- $B^o \to K^{*o}\gamma$ and
- $B^o \to \rho^o\gamma$.

Figure 11.16 shows the p_t distribution (relative to the beam) of the single photons in generic $B-\bar{B}$ events. This can be compared with the p_t distribution of photons from $B^o \to K^{*o}\gamma$ shown in chapter 4. 85% of the signal photons have p_t greater than 1.0 GeV/c while 97% of the remaining photons are below 1 GeV/c.

This kind of cut works to some extent, but less well, in the study of decays with one π^o and a quasi two body hadronic resonance. An example of this is $B^o \to K^{*o}\pi^o$ or $B^o \to \rho^o\pi^o$. Here the p_t of the π^o is the same as the p_t of the single γ in $K^{*o}\gamma$ so the p_t of the individual

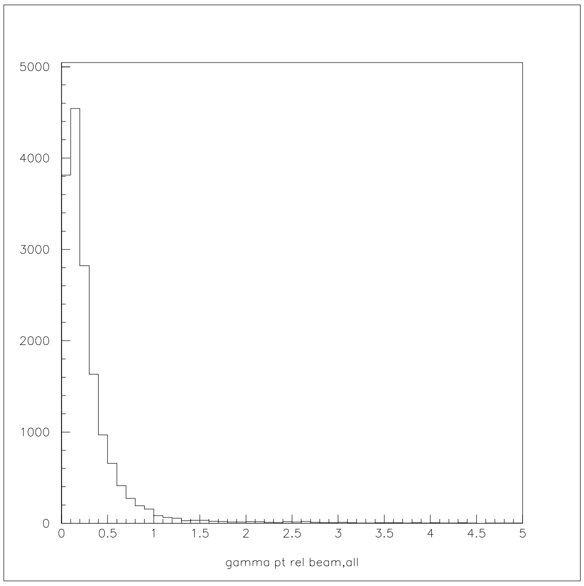

Figure 11.16: The p_t distribution (relative to the beam) of the single photons from all photons in B events.

photons will be lower. Cuts on the p_t of the individual photons or of the π^o relative to the beam will still help to reject background but the effect is not as large as for $K^{*o}\gamma$.

When the π^o is a daughter of the hadronic resonance in a quasi two body decay, such as $B^o \to \rho^+\pi^-$, the π^o and its daughter photons are even closer kinematically to the photons in the underlying event so kinematic cuts are even less effective in this case. This can be seen by comparing the p_t of photons from $B^o \to \rho^+\pi^-$ in Fig. 4.26 with Fig. 11.16.

A second approach uses our excellent measurement of the B direction. The primary vertex is measured by fitting an average of about 10 charged tracks. In B decays which contain at least two charged tracks, the secondary vertex is reconstructed with high efficiency and accuracy. The line connecting the primary and secondary vertex measures the B direction with accuracies of 10-20 mr. The total momentum vector of the charged daughters and the B direction define a plane in which the missing neutral must lie and the B direction defines a line with respect to which the neutral particle's p_t must be equal in magnitude and opposite in direction to the total charged particle p_t. Photons which are not daughters of the B of interest but come from the underlying event or another B or D decay in the event will generally not satisfy this p_t balance requirement. Similarly, if the B decay is really an example of a decay mode with more than one missing neutral or a missing charged track (due to being out of the acceptance or a reconstruction failure), it will generally not satisfy the p_t balance requirement. We have shown that, for all choices of requirements on the calorimeter which satisfy our other requirements, the calorimeter's contribution to the p_t-balance resolution is small compared to the contribution due to the finite position resolution of the vertex detector.

A final defense against the remaining combinatoric background is mass resolution. We have discussed this in chapter 4. Widths of mass distributions are predicted to be 40-50 MeV/c^2. They are dominated by the uncertainty on the measurement of the photon's momentum and are generally factors of 2.5 to 3 worse than for all charged states.

11.5.3 $K^{*o}\gamma$ Analysis Cuts

We used the standard MCFast analysis and vertexing packages for the charged tracks and the MCFast parametrized calorimeter simulation described above. We also used the full BTeV Level 1 trigger simulation. The requirements we placed on events were:

- that it pass the experiment trigger;
- A good primary vertex with at least three tracks and χ^2 per degree of freedom of less than 1.5;
- A neutral combination of a charged K and a charged π which are not included in the primary vertex and which make a good fit to a common vertex with χ^2 less than 3;
- K-π invariant mass between 0.840 GeV/c^2 and 0.940 GeV/c^2;
- $\frac{L}{\sigma_L}$ greater than 3;
- A photon with p_t relative to the beam of greater than 1 GeV/c
- That the photon satisfy a momentum balance requirement with respect to the direction of the B, as determined from the line connecting the primary vertex with the K-π vertex; and
- No other charged track which is unassigned to the primary can form a vertex with the K-π with χ^2 of less than 12.0.

11.5.4 Signal Properties

The invariant mass distribution of the $K-\pi-\gamma$ combinations satisfying all these requirements is shown in Fig. 11.17. The photon p_t is shown in Fig. 11.18. Table 11.4 shows the average values of some quantities of interest to the analysis.

Table 11.4: Average Properties of Signal Events Surviving All Analysis Cuts

Quantity	Value
Mean B Energy	65.5 GeV
Mean Photon Energy	24.8 GeV
Mean Photon Transverse Momentum	3.0 GeV/c
Mean $\frac{L}{\sigma_L}$	11.4

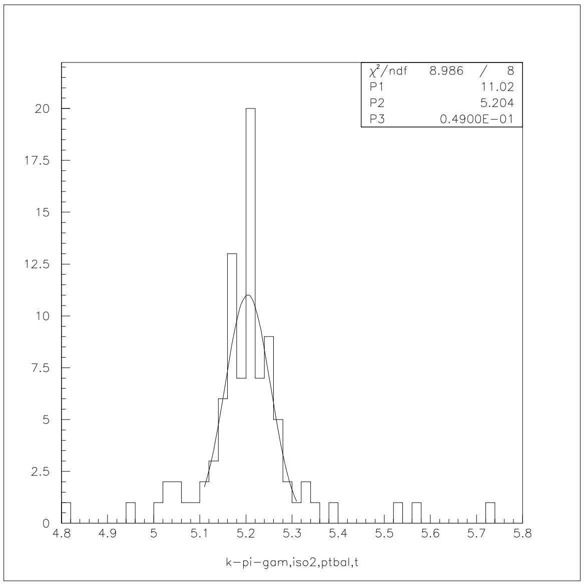

Figure 11.17: Invariant mass spectrum of $K^-\pi^+\gamma$ for events passing the trigger and all analysis cuts. The fit is to a Gaussian and has a σ of 49 MeV/c^2.

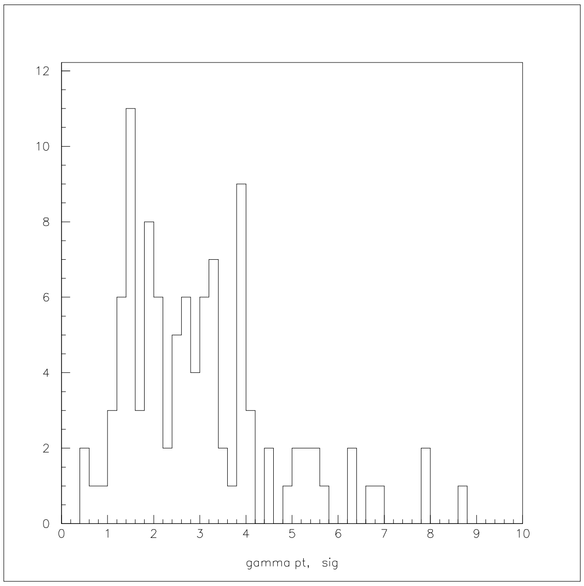

Figure 11.18: p_t spectrum of photons from $K^-\pi^+\gamma$ combinations which pass the trigger and all analysis cuts.

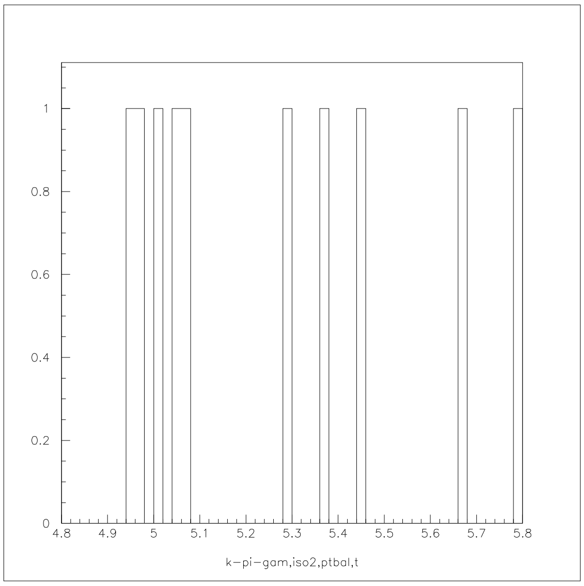

Figure 11.19: Invariant mass spectrum of $K^-\pi^+\gamma$ combinations from background events which pass the trigger and all analysis cuts.

11.5.5 Backgrounds

11.5.5.1 Background from generic B events

The background is calculated as described above. The 400,000 events (out of 20,000,000) surviving at the event generator level are run through MCFast and the identical analysis used for obtaining the signal, described above. The result for the $K^{*o}\gamma$ invariant mass distribution is shown in Fig 11.19.

11.5.5.2 Background from $B^o \to K^{*o}\pi^o$

There is one additional background that we have studied. In the decay $B^o \to K^{*o}\pi^o$, occasionally one photon from the π^o decay will take almost all the energy. Given the finite resolution of the calorimeter, the combination of the real K^{*o} and the higher energy photon from the π^o could have an invariant mass that was very close to the B^o mass. The other photon will have very small energy. If we could detect the soft photon, we could in principle pair it with the candidate single high energy photon, see that it was consistent with the π^o mass, and reject the combination. However, in the complex environment of the collider and with only partial angular coverage, this is not an efficient approach.

We have studied this background by running a sample of generated $B^o \to K^{*o}\pi^o$ decays through the analysis for $B^o \to K^{*o}\gamma$. The result is shown in Fig. 11.20. The solid line is the $K^{*o}\gamma$ signal. The dashed line is the false signal from $K^{*o}\pi^o$. The relative normalization is based on the PDG branching fraction for $K^{*o}\gamma$ and the PDG upper limit for $K^{*o}\pi^o$. The background is not negligible but is not so large as to threaten our ability to see the signal.

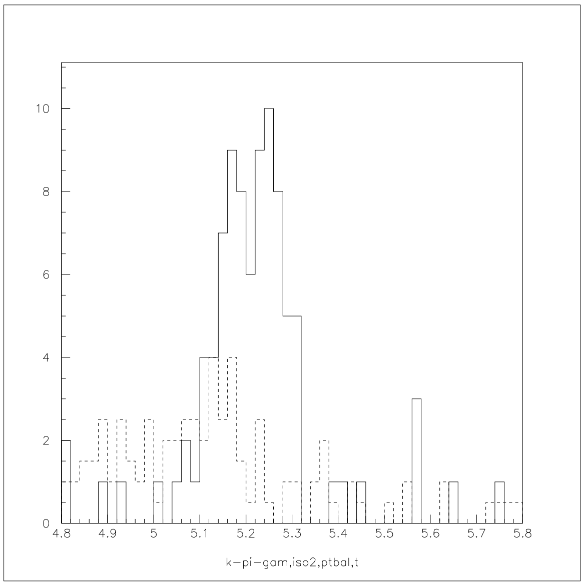

Figure 11.20: Invariant mass spectrum of $K^-\pi^+\gamma$ (solid line) compared to apparent $K^-\pi^+\gamma$ signal (dashed line) from $K^{*o}\pi^o$ events. The relative normalization is explained in the text.

We have not made any attempt to try to suppress it. Some of it could also be from coalesced photons rather than very asymmetric decays and for that we have rejection power that we have not yet used in this analysis. The implications for the study of $B^o \to \rho^o\gamma$, which has a much smaller branching fraction than $B^o \to K^{*o}\gamma$, of the background from $B^o \to \rho^o\pi^o$ will be studied.

11.5.6 Projections of Signal Size and Background

The signal size for one year of running at the design luminosity is shown in table 11.5.

Table 11.5: Number of Reconstructed $B^o \to K^{*o}\gamma$ per year at design luminosity

Total number of B's	2.0×10^{11}
Total number of B^os	7.0×10^{10}
Total number of $B^o \to K^{*o}\gamma$ per 4×10^{-5} branching fraction	28.0×10^5
Total number of $B^o \to K^-\pi^+\gamma$ $K^{*o} \to K^-\pi^+$ branching fraction	18.7×10^5
Total Number Reconstructed (1.3% efficiency, including trigger)	2.4×10^4

The background can be estimated from the 10 events that survived the analysis described above. The estimate for one year of running at the design luminosity is shown in table 11.6

Table 11.6: Number of Reconstructed Background events per year at design luminosity

Total number of B pairs/year	2.0×10^{11}
Total number of background events in 20,000,000 B pairs, mass between 4.8 and 5.8 GeV/c^2	10
Projected background events/year	1.0×10^{5}
Projected background events/year under B mass peak	2.5×10^{4}

While this calculation needs a number of refinements, it looks possible to achieve very large yields of reconstructed $B^o \rightarrow K^{*o}\gamma$ with a signal to background of no worse than a 'few' to one. The background from $K^{*o}\pi^o$ also looks manageable.

We have written out all events that contribute to the background as well as a larger sample of 'near misses', that is events that survived until the last few cuts. By analyzing these and running larger samples of background events, we hope to improve the background rejection and eventually to apply what we learn to the much harder problem of $B^o \rightarrow \rho\gamma$. We will also study $B_s \rightarrow \phi\gamma$ and $B_s \rightarrow K^{*o}\gamma$.

11.6 $B^o \to \rho\pi$

The measurement of the CKM angle α is beset with difficulties. It now seems that a rather complicated amplitude analysis of the decays

$$\begin{aligned} B^o &\to \rho^+\pi^- & (11.13)\\ B^o &\to \rho^-\pi^+ & (11.14)\\ B^o &\to \rho^o\pi^o & (11.15)\\ & & (11.16) \end{aligned}$$

and their charge conjugates may be the best approach. Since the branching fractions for these decays are small, a tagged time-dependent analysis is required and a detailed multiparameter fit must be performed, a large number of events are needed.

We have begun to study these states in BTeV as part of our investigation of the capabilities of our proposed $PbWO_4$ calorimeter. Below we present some early results on the rates of reconstructed events per year that we might achieve. We employ the same approach that we used in the analysis of the decay $B^o \to K^{*o}\gamma$, which was able to reject the background well enough to cleanly isolate the decay. Here we have not begun the study of the background. Moreover, because one wants to be able to carry out an amplitude analysis rather than just measure a rate, it is desirable to reduce the background to a low level. We do not yet know that the analysis cuts employed here will produce a clean enough signal to extract α. The event yields presented here should be taken as an initial indication of what might be achieved.

Analysis cuts are similar to $B^o \to K^{*o}\gamma$ except that there is no cut on the p_t relative to the beam since it would not be very effective in this case. The planarity and momentum balance requirements are now applied to the π^o in this analysis.

Figure 11.21 shows the invariant mass plot of $\pi^+\pi^-\pi^o$ combinations which satisfy the analysis cuts. We expect the peak to narrow when we employ a more sophisticated shower reconstruction. Table 11.7 gives the estimated rate for 1 year of running for tagged events. We use 4×10^{-5} for the branching fraction since it is consistent with theoretical predictions and used by BaBar [15].

Table 11.7: Number of Reconstructed $B^o \to \rho^+\pi^-$ per year at design luminosity

Total number of B's	2.0×10^{11}
Total number of B^os	7.0×10^{10}
Total number of $B^os \to \rho^+\pi^-$ per 4×10^{-5} branching fraction	28.0×10^5
Total Number Reconstructed (1.0±0.2)% efficiency, including trigger)	2.8×10^4
Total number reconstructed and tagged (includes dilution factor)	2.8×10^3

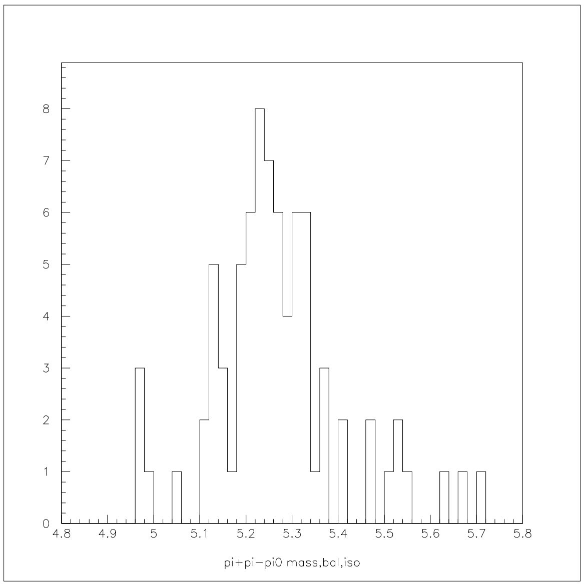

Figure 11.21: The $\pi^+\pi^-\pi^o$ Invariant Mass Distribution for Events Surviving All Analysis Cuts

11.7 Flavor-changing B meson decays

11.7.1 The Physics Significance of Rare B Meson Decays

Within the Standard Model, flavor-changing neutral current decays of b quarks may occur through loop – or penguin– diagrams or box-diagrams. Such decays, which involve small CKM matrix elements and are therefore rare, may be used to extract CKM matrix elements once various long range and perturbative QCD effects are taken into account. If, however, some of these decays occur at a much higher level than predicted by the Standard Model, this would be evidence that there were new particles whose amplitudes could contribute to the loops or boxes. This would provide a path to new physics which is at a higher mass scale than can be probed directly at existing or planned accelerators. Table 11.8 [17] gives a list of some interesting rare decays and their estimated branching fractions.

Table 11.8: Estimated Branching Fractions for Flavor-Changing Neutral Current Decays with Muons and Electrons .

Decay Mode	Est. BR(SM)	Measurements and 90% CL upper limits
$(B_d, B_u) \to X_s\mu^+\mu^-$	$(5.7 \pm 1.2) \times 10^{-6}$	$< 3.6 \times 10^{-5}$
$(B_d, B_u) \to X_d\mu^+\mu^-$	$(3.3 \pm 1.9) \times 10^{-7}$	–
$(B_d, B_u) \to K\mu^+\mu^-$	$(4.0 \pm 1.5) \times 10^{-7}$	$< 0.9 \times 10^{-5}$
$(B_d, B_u) \to K^*\mu^+\mu^-$	$(1.5 \pm 0.6) \times 10^{-6}$	$< 2.5 \times 10^{-5}$
$B_s \to \mu^+\mu^-$	$(3.5 \pm 1.0) \times 10^{-9}$	$< 8.4 \times 10^{-6}$
$B_d \to \mu^+\mu^-$	$(1.5 \pm 0.9) \times 10^{-10}$	$< 1.6 \times 10^{-6}$
$(B_d, B_u) \to X_s e^+e^-$	$(8.4 \pm 2.2) \times 10^{-6}$	–
$(B_d, B_u) \to X_d e^+e^-$	$(4.9 \pm 2.9) \times 10^{-7}$	–
$(B_d, B_u) \to K e^+e^-$	$(5.9 \pm 2.3) \times 10^{-7}$	$< 1.2 \times 10^{-5}$
$(B_d, B_u) \to K^* e^+e^-$	$(2.3 \pm 0.9) \times 10^{-6}$	$< 1.6 \times 10^{-5}$
$B_s \to e^+e^-$	$(8.0 \pm 3.5) \times 10^{-14}$	–
$B_d \to e^+e^-$	$(3.4 \pm 2.3) \times 10^{-15}$	–

11.7.2 Rare Decays in BTeV

Because the Tevatron produces more than 10^{11} b-hadrons per year, we should be able to observe some of these decays and to set stringent limits on others. However, b-physics at the Tevatron also has more sources of background than at e^+e^- B-factories and the sensitivity may be limited by the inability to reject these backgrounds.

Below, we show the results of a study of the decay $B^- \to K^-\mu^+\mu^-$. This decay, according to Table 11.8, occurs with a branching fraction of around $(4.0 \pm 1.5 \times 10^{-7})$. The study is based on simulation runs of 5000 signal events each containing the signal B^- decay and a generic $\bar{b}$-decay and 10^5 background events each of which has both B-mesons decaying semileptonically.

In Fig. 11.22 we show an invariant mass distribution for $B^- \to K^-\mu^+\mu^-$ which also includes background events whose origin is described below. The requirements imposed on events contributing to this plot were determined by the need to achieve very high rejection of the background while maintaining reasonable efficiency. They are:

- A primary vertex consisting of at least 2 tracks with a good χ^2 fit;
- A secondary vertex consisting of three tracks:
    1. one of which is a charged kaon and is required to pass through the RICH and have a momentum greater than 4 GeV/c;
    2. another is a positively charged muon which is required to hit the muon detector and have a momentum greater than 5 GeV/c;
    3. and another is a negatively charged muon which is required to hit the muon detector and have a momentum greater than 5 GeV/c.

  The secondary vertex must have a χ^2 less than 8. The normalized separation, L between the primary vertex and the candidate secondary vertex, L/σ_L, must be greater than 7 and the candidate must satisfy a 'pointback' cut with respect to the primary vertex of less than 2.5 standard deviations.

It is also critical to study the background to this state. The various sources of background are:

- Minimum bias events where three particles conspire to fake a secondary vertex and two of the particles either decay downstream of the magnet or make hadronic showers which leave a signal in the muon detector (hadron punchthrough).
- Charm events with one or more real muons and kaons.
- b-events where portions of the two b-hadrons in the event appear to verticize downstream of the production point. In approximately 1% of all $b\bar{b}$ events both B-hadrons decay semileptonically producing two real muons. In addition, there is a charged kaon in at least one of the b's over 90% of the time.
- More generally, any variety of admixture of B, charm, minimum-bias events, primary interactions and secondary decays, combined with hadronic punchthrough.

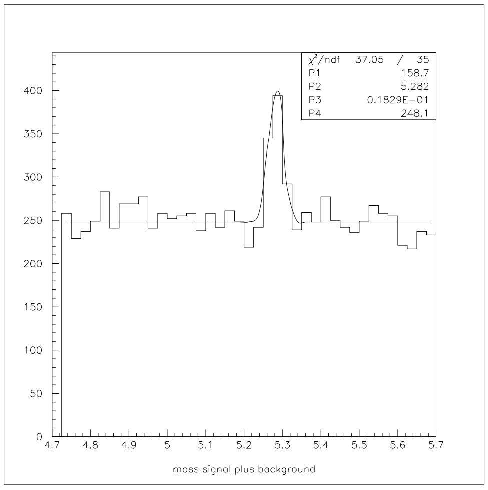

Figure 11.22: Invariant mass spectrum of $K\mu^+\mu^-$ including an estimate of the background from events where both b's decay semileptonically (also obtained with MCFast).

- Fake events from single b decays such as $B^- \to K^-\pi^+\pi^+$ where both pions fake muon signatures by decay or punchthrough. Another possibility is the decay $B^- \to D^o\pi^-$ where the D vertex is not seen as separated from the B vertex and where both pions simulate muons. However, a mass cut on the D will remove this background.

The basic weapons to combat backgrounds are:

- Excellent mass resolution on the final state.
- Excellent discrimination between the primary and secondary vertex which eliminates backgrounds from the minimum-bias events and from the underlying event within a true b-event.
- Excellent 'pointback' resolution between the reconstructed b candidate and the primary vertex which will do much of the work to reject events that have been artificially pieced together from particles from the two separate b's in the event.
- The ability to reject events where other tracks point to the candidate vertex, where some of the tracks in the candidate vertex also point to the primary, or where some of the tracks in the candidate vertex intersect with other tracks not in the primary vertex (i.e. tracks from the associated b).

In addition, the signal-to-background depends on the quality of both the muon detector and the particle identification.

We did not include the decay $B^- \to \psi K^-$ as a background. That decay is large compared to the rare decay being considered here and will interfere with the rare decay and distort the dimuon mass distribution in the vicinity of 3 GeV/c^2. This, however, is a physics contribution and will certainly be observed and studied based on a mass cut on the dimuon. In fact, this state can be used to calibrate the efficiency of the analysis and can be used as a normalization for a measurement of the relative branching fraction.

We have not simulated all sources of background. Our own estimates indicate that the most serious background is from events with pairs of B's which each undergo semileptonic decays. We have analyzed 10^5 simulated events of this type and have a background in the mass plot (4.7 to 5.7 GeV/c^2) of 1 event in 40 bins (which we can make disappear with only a slight adjustment in cuts). We obviously need to run more background events. However, if we scale this result to the correct mass interval and by the correct relative normalization factor, we estimate a background of about 750 events (with a very large error) under a peak of about 300 – or signal to background of 1 to 3 and a statistical significance of 10 standard deviations. We show what this would look like by including this estimated background in Fig. 11.22. We discuss below how to reduce this background further.

The overall efficiency for this state, with cuts designed to achieve good background rejection, is about 2.5%. Table 11.9 gives a calculation of the yield obtained in a one year run at a luminosity of $5\times10^{31}\mathrm{cm}^{-2}\mathrm{s}^{-1}$. We include in this calculation a triggering efficiency of 80% for those events which satisfy all the analysis cuts. This is consistent with what we expect to get from the dimuon trigger (70%) 'or-ed' with the vertex trigger which recovers almost half of what the muon trigger failed to accept.

Table 11.9: Estimate of Yield for $B^\pm \to K^\pm\mu^+\mu^-$

Quantity	Value
Luminosity	$2.0\times10^{32}\mathrm{cm}^{-2}\mathrm{s}^{-1}$
Running Time/year	10^7s
$b\bar{b}$ cross section	100μb
Total $b\bar{b}$ pairs produced	2×10^{11}
Total $B^\pm$	1.4×10^{11}
Branching fraction	4×10^{-7}
Efficiency (cuts above)	2.5%
Total signal events	1400
Events satisfying trigger	1120
Estimated background	3000
Signal to background	0.37
Statistical significance of observation	>> 10 Standard deviations
Uncertainty on branching fraction	5%

There is much work left to be done, especially on understanding and rejecting the backgrounds. However, we have not exhausted all the weapons we have available to defeat these backgrounds. We have not optimized pointback cuts, χ^2 cuts on the secondary vertex, or the L/σ_L cut. Cuts that we have not yet employed include those which reject the event if there are other tracks that intersect the candidate secondary vertex and which reject the event if the daughter tracks of the candidate point either to the primary vertex or intersect with another track that is not in the primary (presumably from the other b in the event). We have also not investigated kinematic cuts to see if any characteristic of the individual particle p_t's or the dimuon mass distribution, or the angular distributions of the particles in the decay rest frame can help discriminate signal from background. Nevertheless, the initial results are very encouraging.

According to the CDF II Technical Design Report [16], CDF expects a signal of 100-300 $B^+ \to \mu^+\mu^- K^+$ events in collider RUN II. The signal-to-background is expected to be better than the 1 to 10 achieved in RUN I. However, CDF, because of its lack of particle identification for tracks above 1 GeV/c, is exposed to background from all the pions in the event conspiring with the muons to create background. In BTeV, because of the RICH, only the kaons can contribute to the background and there are fewer of them. The RICH reduces the background in this final state by about a factor of three, with a negligible loss of signal. BTeV will have intrinsically lower background than detectors without powerful particle identification on most final states. In light of the discussion above, it is reasonable to say BTeV's sensitivity for detecting rare B decays is quite a bit better than CDF's.

11.8 B_s Mixing with $B_s \to D_s^- \pi^+$ and $B_s \to \psi \bar{K}^{*0}$

As discussed in section 1.10.1 the measurement of B_s mixing allows a determination of $|V_{ts}/V_{td}|$, which corresponds to one side of the B unitarity triangle. While the theoretical discussion was given in terms of the mass splitting between the light and heavy B_s mass eigenstates, Δm_s, the discussion here will be in terms of x_s, where $x_s = \Delta m_s/\Gamma$.

In this section the x_s reach of BTeV will be demonstrated. This study was carried out in several steps, the first step being an MCFast based simulation of the BTeV detector, which was run on samples of both signal and background events. The output of this step was treated as real data and passed through a physics analysis program to determine the yield, the time resolution and the signal-to-background ratio in each mode. All of the preceding material is covered in section 11.8.1. This information was then passed to a separate program which computed the x_s reach; this program is discussed in section 11.8.2.

11.8.1 Yields, Resolutions and Signal-to-Background Ratios

The mode for which BTeV has the most sensitivity to x_s is $B_s \to D_s^- \pi^+$, where the D_s^- decays either by $D_s^- \to \phi\pi^-$, $\phi \to K^+K^-$, or by $D_s^- \to K^{*0}K^-$, $K^{*0} \to K^+\pi^-$. Both of these D_s^- modes have narrow intermediate states and characteristic angular distributions, which can be used to improve the signal-to-background ratio. Another mode with good x_s sensitivity is $B_s \to \psi\bar{K}^{*0}$, $\psi \to \mu^+\mu^-$, $\bar{K}^{*0} \to K^-\pi^+$. Although this mode is Cabibbo suppressed, many other factors are in its favor: the final state consists of a single detached vertex; it has a relatively low multiplicity; the state is triggerable with several independent strategies, including impact parameter triggers, secondary vertex triggers and muon or di-muon triggers [19]. While this mode does not have the reach of $D_s^-\pi^+$ it does cover much of the range and it provides a powerful check with partly independent systematics.

In the simulation step, $p\bar{p} \to b\bar{b}X$ events were generated using Pythia 6.125. All charmed and bottom hadrons were decayed using QQ [18]. In order to simplify the analysis, all B_s mesons were forced to decay into the signal channel and all $\bar{B}_s$ mesons were permitted to decay generically, but with mixing disabled and with the charge conjugate of the signal channel excluded. The effect of mixing is included in the final calculation of the x_s reach, in section 11.8.2.

In the $D_s^-\pi^+$ analysis, the first step was to impose track quality requirements on each reconstructed track in the event. All tracks were required to have a minimum number of hits, which is a simplified model of the fiducial requirements of the tracking system. No further requirements were placed on $\pi^\pm$ candidates. All $K^\pm$ candidates were required to lie within the fiducial acceptance of the RICH; any track which had hits in the forward tracking station which is located between the RICH and the EM Calorimeter, and which had a momentum in the range $3.0 \leq p \leq 70$ GeV/c, was deemed to satisfy the fiducial requirements. It was assumed that all tracks inside the fiducial acceptance of the RICH could be correctly identified. The next step in the simulated analysis was to form all $K^+K^-\pi^-$ combinations in an event. These combinations were fitted to a common vertex and a combination was retained as a D_s^- candidate provided the χ^2 of the vertex fit was acceptable and provided the combination passed the mass and angle requirements of either the $\phi\pi^-$ or the $K^{*0}K^-$ hypothesis. Each D_s^- candidate was then vertexed with each remaining π^+ candidate in the event and, provided the χ^2 of the vertex fit was acceptable, the $D_s^-\pi^+$ combination was retained as a B_s candidate. Before computing the mass of the B_s candidate, the mass of the D_s^- candidate was constrained to its PDG value.

For each event, a primary vertex was defined by looking at the generator information to identify the tracks that belonged in the primary vertex. These tracks were then fitted to a common vertex. This procedure gave the resolution of the primary vertex on an event by event basis. A separate study showed that the precision of the BTeV apparatus is sufficiently good that primary vertex pattern recognition will be highly efficient and of high purity. Once the primary vertex has been found, further requirements were placed on the B_s candidates. They were required to have a detachment from the primary vertex of $L/\sigma_L > 4.0$, where L is the decay length of the B_s candidate. They were required to have an impact parameter with the main vertex, d, of less than $3\,\sigma_d$ and to have a p_T balance along the line connecting the primary and secondary vertices of less than 1.0 GeV/c. The daughter D_s^- candidate was required to have $L/\sigma_L > 4.0$.

Some interesting quantities for B_s candidates are shown in Fig. 11.23. In part a) we see that the mass resolution on the B_s is 19.2 ± 0.8 MeV/c^2. Part b) shows the resolution on the proper decay time; the mean of this distribution, 50 fs, will be used, below, in the calculation of the x_s reach. Part c) illustrates the main power of the BTeV apparatus, its excellent vertex resolution. Finally, part d) illustrates one of the important background suppression cuts; background combinations which pass the other cuts will usually not point back to the primary vertex.

In order to measure x_s, it is necessary to tag the flavor with which the B_s meson was created. In the BTeV Expression of Interest [9] it was argued that opposite side $K^\pm$ tagging will have an efficiency of 0.12 with a mistag fraction of 0.25 and that opposite side muon tagging will have an efficiency of around 0.03, also with a mistag fraction of 0.25. These tags correspond to $\epsilon D^2 = 0.075$. We expect that same side tagging of the B_s can be a rather clean tagging method; however we have not yet investigated this tagging method in sufficient detail to use it in this analysis. As discussed in section 11.3, it is expected that the total tagging power will reach $\epsilon D^2 = 0.10$. The additional power will come from tags with much higher efficiency but with much higher mistag fractions. For purposes of this work, only the clean tags will be considered.

Finally, the BTeV Level 1 trigger simulation was run on the $B_s \to D_s^-\pi^+$ sample. Using the standard requirement that there be two tracks detached by at least $4\,\sigma$ and with $p_T > 0.5$ GeV/c^2, we find that 60% of the events which pass all analysis cuts also pass the trigger.

Table 11.10 shows a breakdown of the efficiencies measured by MCFast, as well as listing all assumptions which went into the computation of the yield. In one year we expect that 16,100 events will survive all analysis cuts, have their birth flavor tagged and be triggered.

It is believed that the dominant source of backgrounds will be events of the form $B \to D_s^- X$, where B may be any of B_u, B_d or B_s. The background combinations arise

Quantity	Value	Yield (Events/year)
Luminosity:	2×10^{32} cm^{-2}s^{-1}	
One Year:	10^7 s	
$\sigma_{b\bar{b}}$:	100 μb	
$\mathcal{B}(B_s \to D_s^- \pi^+)$:	3.0×10^{-3}	
$\mathcal{B}(D_s^- \to \phi\pi^-)$:	0.030	
$\mathcal{B}(D_s^- \to K^{*0}K^-)$:	0.036	
$\mathcal{B}(\phi \to K^+K^-)$:	0.49	
$\mathcal{B}(K^{*0} \to K^+\pi^-)$:	0.67	
$\mathcal{B}(\bar{b} \to B_s)$	0.13	6,210,000
ϵ(Geometric)	0.08	
ϵ(Analysis cuts : $\phi\pi^-$)	0.40	
ϵ(Analysis cuts : $K^{*0}K^-$)	0.33	
ϵ(Trigger)	0.60	108,000
ϵ(Tag)	0.15	16,100
Mistag fraction	0.25	
S/B	3:1	
σ(Proper Decay time)	50 fs	

Table 11.10: Projected Yield for $B_s \to D_s^- \pi^+$ in one year of BTeV running. The numbers in the third column give the expected yield when all of the factors down to and including that line have been considered. The branching fraction $\mathcal{B}(B_s \to D_s^- \pi^+)$ was estimated to be the same as $\mathcal{B}(B_d \to D^- \pi^+)$. The value for $\mathcal{B}(\bar{b} \to B_s)$ was obtained from [14]. All efficiencies are multiplicative. The tagging efficiency and mistag fraction are quoted from the sum of clean tagging modes only.

when a true D_s^- combination is combined with some other track in the event. When 1 million $B \to D_s^- X$ events were passed through MCFast and the full analysis chain only 8 entries remained in a mass window 6 times larger than the mass window used to select signal B_s candidates. From this we estimate that the signal-to-background ratio in this channel is 8.4:1. We have not yet investigated the background from direct charm production; while direct charm production is about 10 times more frequent than production of charm from B decay, we believe that the required two vertex topology will greatly reduce the direct charm background. In the end we expect that background from $B \to D_s^- X$ will dominate. We have yet to do a full treatment of the impact of multiple interactions in one beam crossing. In the end we make a conservative estimate that we will achieve a signal-to-background ratio of no worse than 3:1.

The analysis of the $\psi\bar{K}^{*0}$ mode proceeded similarly to that of the $D_s^-\pi^+$ mode and only the important differences will be summarized here. In order to be considered a muon candidate, a track was required to have a momentum $p > 5.0$ GeV/c and to penetrate the hadron filter, thereby leaving hits in the most downstream muon chambers. In this decay mode the topology is simpler, with all four tracks coming from a single vertex. A $\mu^+\mu^-K^-\pi^+$ combination was retained if the confidence level of fitting all four tracks to a single vertex was greater than 0.005. It was also required the that resonant substructure requirements be satisfied. Combinations were considered for further analysis provided $L/\sigma_L > 10$ and $d < 3\sigma_d$. Each of the four B_s grand-daughters were required to have an impact parameter with the primary vertex, $d > 2\,\sigma_d$. Candidates with poor time resolution were rejected by demanding $\sigma_t \leq 0.09$ ps. After constraining the mass of the ψ to its PDG value, the mass resolution of the B_s was determined to be 12.0 ± 0.6 MeV$/c^2$. For the $\psi\bar{K}^{*0}$ mode, the mean resolution on the proper decay time was found to be 38 fs.

The BTeV Level 1 trigger simulation was run on the $\psi\bar{K}^{*0}$ sample, using the same trigger conditions as described above. We find that, of the candidates which pass all analysis cuts, $69 \pm 3\%$ also pass the trigger; the error is purely statistical. However this mode can also be triggered by a single muon or a di-muon trigger and we estimate that the total trigger efficiency will be approximately 85%.

By far the dominant background is expected to come from decays of the form $B \to \psi X$, $\psi \to \mu^+\mu^-$. An MCFast simulation of 500,000 such decays gives a predicted signal-to-background level of about 2:1. Some sources of background which one might at first think to be important turn out not to be a problem. First, the more copious $B_s \to \psi\phi$ final state is not a significant source of background because of the excellent particle ID provided by the RICH system. Second, the mass resolution is sufficient to separate the much more copious decay $B_d \to \psi\bar{K}^{*0}$.

Finally, the expected yield can be increased by a factor of at least 50% by using the mode $\psi \to e^+e^-$. This mode will have an efficiency for secondary vertex triggers which is comparable to that for $\psi \to \mu^+\mu^-$ and, an as yet unspecified, electron trigger is part of the BTeV baseline design.

Table 11.11 shows a breakdown of the efficiencies measured by MCFast, as well as listing all assumptions which went into the computation of the expected yield. In one year we expect that 1030 events will survive all analysis cuts, have their birth flavor tagged and be triggered.

11.8.2 Computation of the x_s Reach

The final step in the study was to use a mini-Monte Carlo [20] to study the x_s reach of BTeV. This mini-Monte Carlo generates two lifetime distributions, one for mixed events and one for unmixed events, smears the distributions and then extracts a measured value of x_s from a simultaneous fit the two distributions. The time smearing is Gaussian, using the mean time resolutions determined above. The model includes the effects of mistagging, background under the signal, and the minimum time cut which is implied by the L/σ_L cut. It is assumed that the lifetime distribution of the background is an exponential with the same mean lifetime as that of the B_s.

Figures 11.24a) and b) show the proper time distributions which result from one run of

Quantity	Value	Yield (Events/year)
Luminosity:	2×10^{32} cm^{-2}s^{-1}	
One Year:	10^7 s	
$\sigma_{b\bar{b}}$:	100 μb	
$\mathcal{B}(B_s \to \psi \bar{K}^{*0})$:	8.5×10^{-5}	
$\mathcal{B}(\psi \to \mu^+\mu^-)$:	0.061	
$\mathcal{B}(\bar{K}^{*0} \to K^-\pi^+)$:	0.667	
$\mathcal{B}(\bar{b} \to B_s)$	0.13	180000
ϵ(Geometric)	0.18	
ϵ(Analysis cuts)	0.17	5508
ϵ(Trigger) Tracking only	0.60	
ϵ(Trigger) Total	0.85	4680
ϵ(Tag)	0.15	700
Include $\psi \to e^+e^-$		1030
Mistag fraction	0.25	
S/B	2:1	
σ(Proper Decay time)	38 fs	

Table 11.11: Projected Yield for $B_s \to \psi \bar{K}^{*0}$ in one year of BTeV running. The numbers in the third column give the expected yield when all of the factors down to and including that line have been considered. The estimate for $\mathcal{B}(B_s \to \psi \bar{K}^{*0})$ was obtained from [19] and that for $\mathcal{B}(\bar{b} \to B_s)$ was obtained from [14]. The trigger efficiency is quoted as a fraction of those events which pass the analysis cuts. The tagging efficiency and mistag fraction are quoted from the sum of clean tagging modes only.

the mini-Monte Carlo for a generated value of $x_s = 40$. The simulation is for the decay mode $B_s \to D_s^- \pi^+$ for one year of BTeV running; that is for 16,100 signal events, with $S/B = 3:1$, a time resolution of 50 fs, and a 25% mistag rate. It was also required that the smeared decay time be greater than 200 fs, which simulates the cut of $L/\sigma_L > 4$. Part a) shows the proper time distribution for unmixed decays while part b) shows the distribution for mixed decays. Part c) of the figure shows, as a function of x_s, the value of the unbinned negative log likelihood function computed from the simulated events. A step of 0.5 in the negative log likelihood function determines the 1 σ error bounds and a line is drawn across the figure at the level of the 5 σ error bound. A clear minimum near the generated value of x_s is observed and the likelihood function determines the fitted value to be $x_s = 40.0 \pm 0.04$.

The error returned by the fit was checked in two ways. First, an ensemble of mini-Monte Carlo experiments was performed and the errors were found to correctly describe the dispersion of the measured values about the generated ones. Second, the errors returned by the fit were found to be approximately equal to the Cramer-Rao minimum variance bound [20].

The mini-Monte Carlo also showed how the limiting x_s sensitivity of the experiment is approached. As the number of events in a trial is reduced, the negative log likelihood function becomes more and more ragged and the secondary minima approach the significance of the global minimum. Eventually there are secondary minima which reach depths within 12.5 units of negative log likelihood (5σ) of the global minimum. When this happens in a sufficiently large fraction of the trials, one must conclude that only a lower limit on x_s can be established. In the region of the parameter space which was explored, the absolute error on x_s was approximately 0.1 when this limit was reached. This was independent of the generated value of x_s.

It is awkward to map out the x_s reach of the apparatus by running a large ensemble of mini-Monte Carlo jobs. Instead the following automated procedure was used. Following ideas from McDonald [21], the sum over events in the likelihood function was replaced with an integral over the parent distribution. Because the parent distribution does not have any statistical fluctuations, the fluctuations in the likelihood function are removed, leaving only the core information. An example of such a likelihood function is shown in Fig. 11.25.

A likelihood function computed in this way has the property that it scales linearly with the number of events being simulated. This can be stated formally as follows. Let x_0 denote the generated value of x_s and let $\mathcal{L}(x; x_0, N)$ denote the value of the likelihood function, evaluated at x, for a sample which has a true value of x_0 and which contains N events. Then,

$$\mathcal{L}(x; x_0, N) \quad = \quad N\mathcal{L}(x; x_0, 1) \tag{11.17}$$

Now, one can define the significance of the minimum, n, as,

$$n^2 \quad = \quad 2.0\, N \left[\mathcal{L}(\infty; x_0, 1) - \mathcal{L}(x_0; x_0, 1)\right]. \tag{11.18}$$

For practical purposes ∞ was chosen to be 160. If we did not have to worry about the missing statistical fluctuations it would be normal to define a significant signal as $5\,\sigma$, or

$n^2 = 25$. Instead, we defined significance, somewhat arbitrarily, as $n^2 = 31.25$, which allows for the usual $5\,\sigma$ plus a downwards fluctuation of up to $2.5\,\sigma$ anywhere else in the plot. Equation 11.18 was solved for N, which was then converted into the running time required to obtain a measurement of $n\,\sigma$ significance. This procedure was repeated for many different values of x_0 to obtain Fig. 11.26. The solid line shows, for the $D_s^- \pi^+$ mode, the number of years needed to obtain a $5\,\sigma$ significant measurement, where "$5\,\sigma$" means $n^2 = 31.25$. Had we ignored the missing fluctuations and kept $n^2 = 25$, the x_s reach between 1 and 3 years would have been shifted higher by about 3 or 4 units of x_s. For small values of x_s the difference is not visible. The dashed line shows the same information for the $\psi \bar{K}^{*0}$ mode, for which the effect of setting $n^2 = 31.25$ is similar.

Inspection of Fig. 11.26 shows that, using the $D_s^- \pi^+$ mode, BTeV is capable of observing all x_s less than 60 in one year of running. Moreover there are two changes in the pipeline which we expect will improve this reach: we expect to be able to build pixel detectors which have less mass than those in the present design and we have not yet full exploited the tagging power of BTeV.

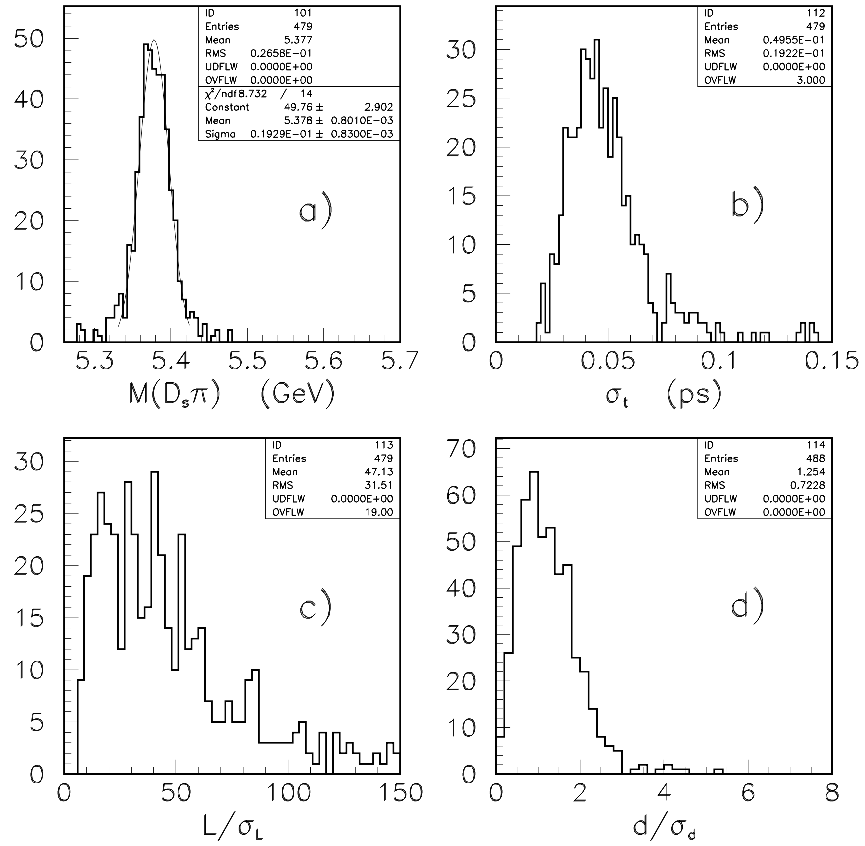

Figure 11.23: Distributions of properties of $B_s \to D_s^- \pi^+$ candidates. For candidates which survive all cuts, part a) shows the invariant mass of the B_s candidate, part b) shows the resolution on the proper decay time and part c) shows the detachment of the B_s from the primary vertex. Part d) shows the significance of the impact parameter, d, of the B_s candidate with the primary vertex; for the final selection it was required that $d/\sigma_d \leq 3.0$.

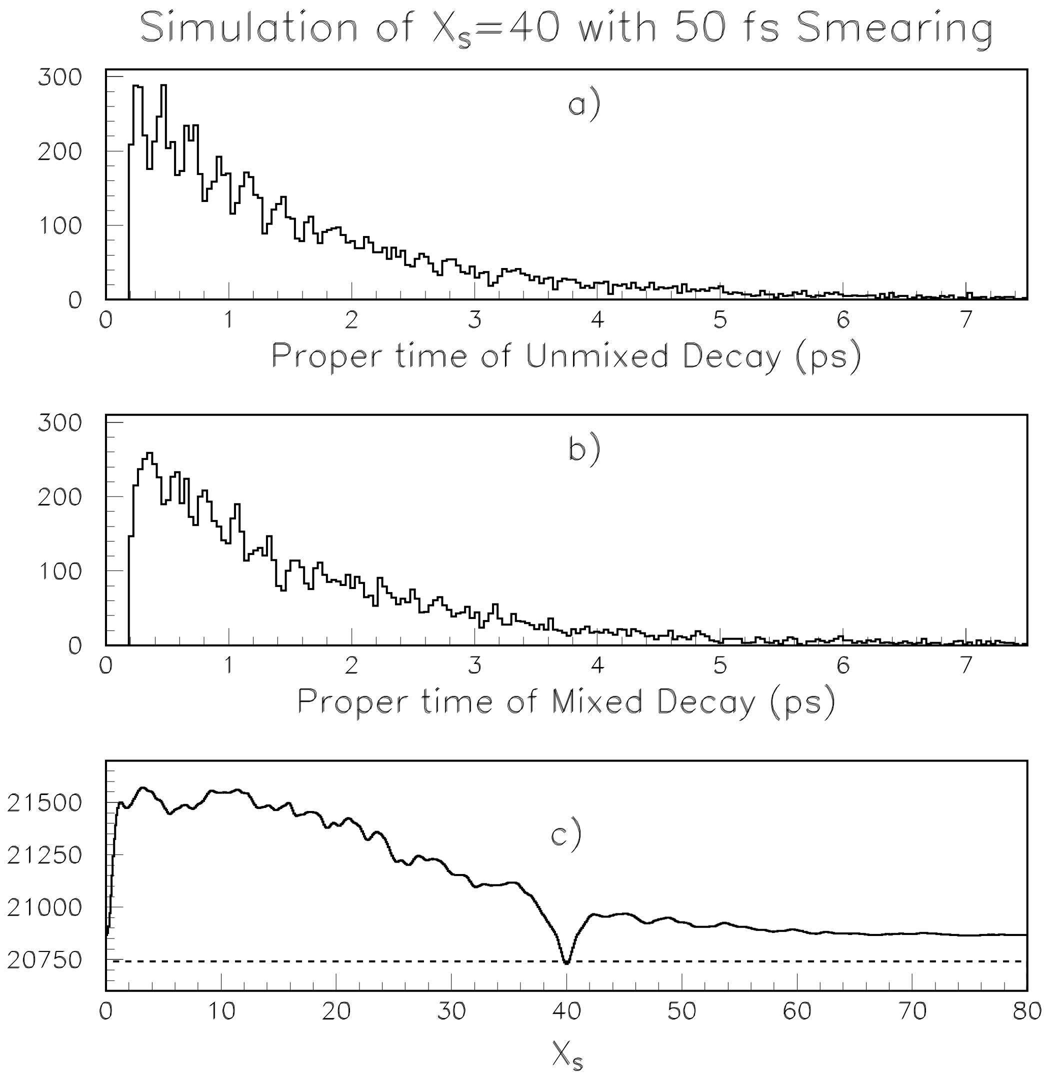

Figure 11.24: Mini-Monte Carlo Proper Lifetime plots of a) unmixed and b) mixed decays for one BTeV year of $B_s \to D_s^- \pi^+$ with $x_s = 40$, a mistag fraction of 0.25, a time smearing of 50 fs, a signal-to-background ratio of 3:1 and a minimum time cut of 200 fs. The oscillations are prominent. Part c) shows the negative log likelihood as a function which was obtained from the entries in parts a) and b). A prominent minimum is seen at the generated value of x_s. The dashed line marks the level above the minimum which corresponds to 5 σ significance.

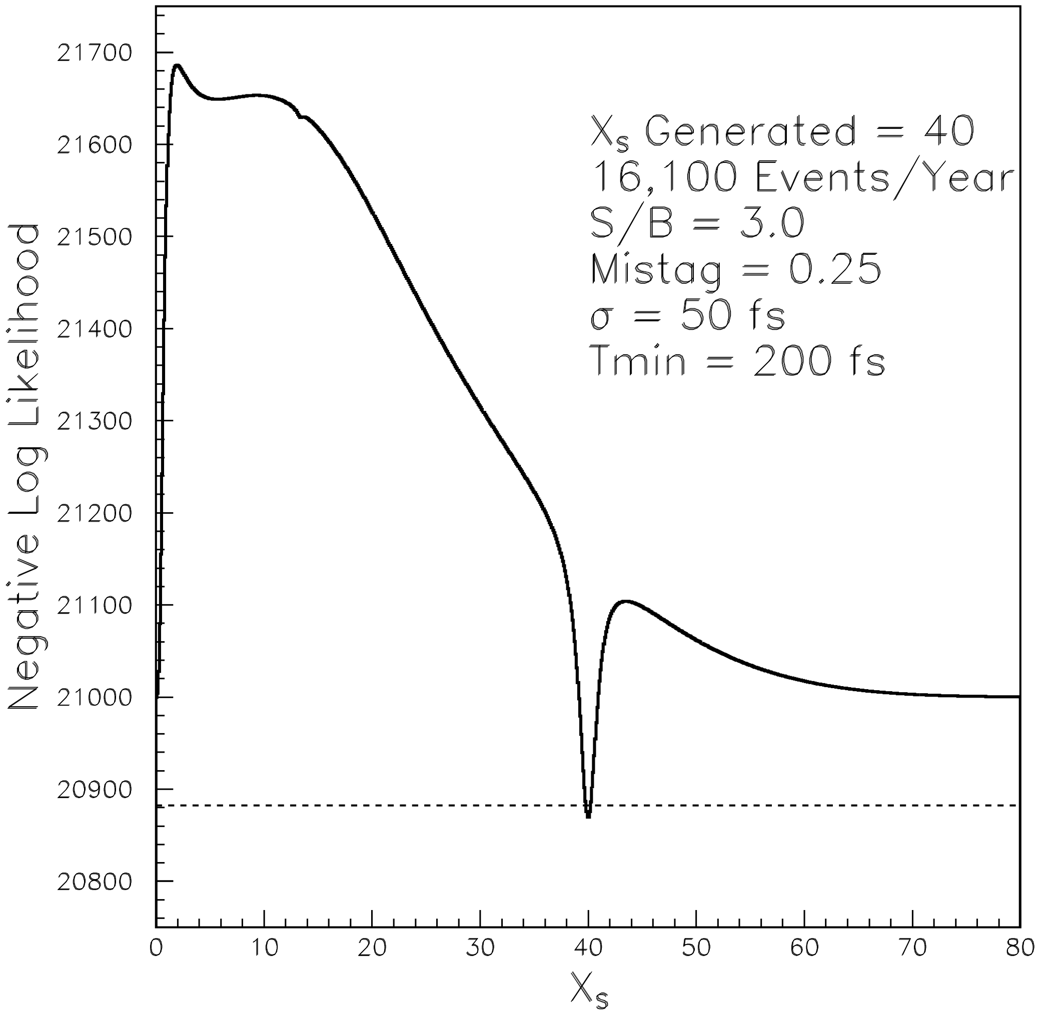

Figure 11.25: The same likelihood function as in part c) of the previous figure but using the calculation described in the text. The overall shape is the same but the statistical fluctuations have been removed. There is also an overall level shift which is related to the goodness of fit in the previous figure.

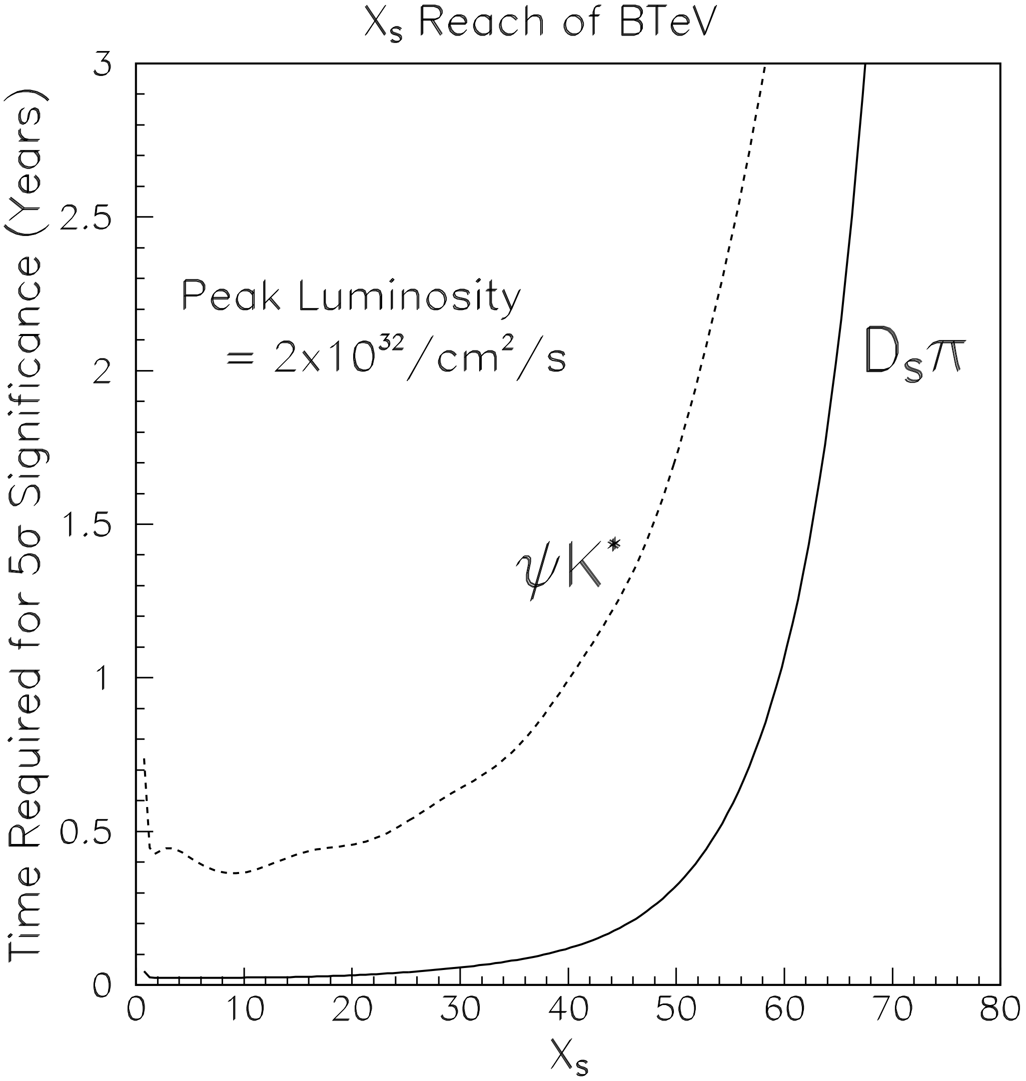

Figure 11.26: The x_s reach of the BTeV detector. The curves indicate the number of years of running which are required to make a measurement of x_s with a statistical significance of $5\,\sigma$. The curves are shown for two different decay modes.

11.9 Charm Physics with the BTeV Detector

Searches for mixing, CP violation, and rare and standard model forbidden decays in the charm sector (as discussed in chapter 2) provide a sensitive and possibly unique window to physics beyond the standard model. At a luminosity of $2 \times 10^{32}\text{cm}^{-2}\text{s}^{-1}$ the Tevatron produces on the order of 2×10^{12} charm quark pairs ($c\bar{c}$) a year (although the $c\bar{c}$ cross section at $\sqrt{s}$=2 TeV is not well known, a relatively conservative estimate for it is 1 mb). Such a sample represents an opportunity unavailable anywhere except at hadron colliders, although this potential has yet to be tapped.

Charm physics simulation studies are not as advanced as the beauty studies presented previously in this report. The simulations presented here used a detector geometery with less material in the pixels and tracking stations than we used for the b studies, and did not use the square hole pixel geometry that substantially improves the acceptance. We estimate that the efficiencies will not change by more than $\pm 10\%$. In addition, no effort has yet been made to optimize triggers for charm modes. These studies are beginning now.

As a first step in studying charm physics in collider mode, we have computed the geometrical and tracking acceptances of the baseline BTeV detector (see Part II) for several charm meson decay modes using the MCFast package. We are interested in: (i) the inclusive acceptance (or "single charm"), which refers to the probability to detect all daughters of a charm or anti-charm meson, and (ii) the "associated" acceptance, defined as the probability to detect both secondary (charm and anti-charm) vertices.

At the current time we have only considered all-charged final states such as $D \to K^- + n\pi$ and $D^0 \to K^+K^-$. The recoiling anti-charm (or charm) hadron decays according to PDG branching ratio values. The QQ package has been used to simulate these decays. To define our acceptance, we require that each daughter in a decay leave a minimum number of hits in the spectrometer, which directly reflects our ability to reconstruct the corresponding tracks. To be considered "accepted", a track must produce at least 4 hits in the vertex detector (which implies that it must pass through at least two stations) and 6 hits in the forward tracker.

The inclusive acceptance for $D^0 \to K^-\pi^+$, $D^+ \to K^-\pi^+\pi^+$ and $D^0 \to K^-\pi^+\pi^-\pi^+$ is 24%, 15%, and 11%, respectively. While the acceptance does depend on decay multiplicity, it does not depend strongly on the strangeness content of the daughter tracks (e.g., kaons vs pions), so the acceptance for Cabibbo suppressed decays is similar to that for Cabibbo favored ones of equal multiplicity. The acceptance for $D^{*+} \to D^0\pi^+$, $D^0 \to K^-\pi^+, K^-\pi^+\pi^-\pi^+$ is noticeably lower than the acceptance for final states of the same multiplicity, due to the much softer momentum of the "bachelor" pion from the D^{*+} decay. This can be mitigated by removing the requirement that this pion reach the forward tracker system. The resolution in $\Delta M = M(D^*) - M(D^0)$ deteriorates due to the diminished momentum resolution for bachelor pions not tracked in the forward tracker (see Fig. 11.27). The acceptance for these decays is approximately 17%

The associated acceptance is defined to be the probability that one decay vertex is fully reconstructed and the second decay vertex is at least partially reconstructed. To calculate

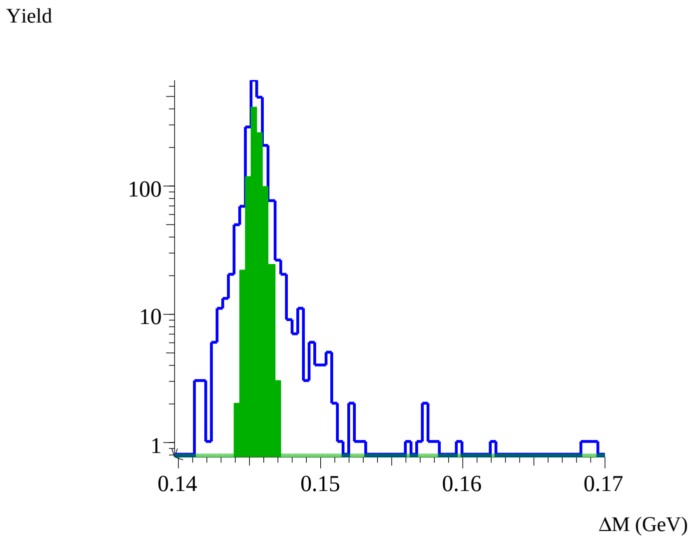

Figure 11.27: The $\Delta M = M(D^*) - M(D^0)$ mass plot, as estimated by the MCFast package, for the baseline detector, where the D^0 decays to $K^-\pi^+$ and $K^-\pi^+\pi^-\pi^+$ (with relative branching ratios according to PDG values). The solid shaded histogram refers to the case where the soft pion from the D^* decays is detected by the forward spectrometer, while the solid line histogram refers to the case where this soft pion is detected only by the pixel detector.

this acceptance we again use Monte Carlo events where one daughter decays to all-charged tracks, and the other daughter decays according to PDG branching ratios. We then require that the all-charged track mode be fully reconstructed (just as in the inclusive calculation above). The other charm decay must have at least two tracks reconstructed. These tracks are required to leave at least 9 hits in the vertex and forward trackers. The acceptances for the $K^-\pi^+$, $K^-\pi^+\pi^+$ and $K^-\pi^+\pi^+\pi^-$ modes are 15%, 12% and 5%, respectively. These acceptances are typically an order of magnitude higher than those observed in fixed target experiments, simply because of the strong kinematical correlation between the $c\bar{c}$ pair (if the charm meson is boosted into one of the arms of the spectrometer, it is likely that the anti-charm also gets a similar boost and is observed in the same arm). One of the benefits is cleaner primary vertices than in a fixed target configuration.

11.9.1 Direct CP Violation in the Charm Sector

In order to estimate the sensitivity of the BTeV spectrometer for a possible observation of Direct CP violation in the charm sector, we have studied in more detail the acceptance and background rejection capabilities for a specific Cabibbo-suppressed decay mode: $D^*(2010)^+ \to D^0\pi^+$, $D^0 \to K^+K^-$. The geometrical acceptance of the vertexing and tracking systems has already been presented in the previous subsection. Now, we concentrate on vertexing cuts, overall sensitivity and systematic errors.

Following the constrained vertex reconstruction algorithm, used by the experiment E687 [1] [23], K^+K^- tracks with a relatively large invariant mass are first selected in the event. These are MCFast "offline tracks", i.e. simulated reconstruction tracks for which we have a covariance matrix allowing us to compute a vertex error and χ^2. Note that such tracks are not the outcome of a full pattern recognition package in the forward tracker and the pixels. However, based on studies done for the pixel-based trigger, we know that the level of confusion in this vertex detector is not likely to be a limitation, thanks to its high granularity.

In addition to a minor vertex quality cut on the D^0 candidate vertex, the charged kaons are required to be positively identified as such by the Cerenkov system. We have assumed 97.5% percent positive identification for momenta between 3 and 70 GeV/c and no identification outside this range. Under these conditions, the effective D^0 acceptance is 17.4% (the tracking acceptance for this final state is 25%).

The soft pions from the D^* decays are not required to be reconstructed by the forward tracker and are mostly reconstructed by the vertex detector. At least six hits are required on this soft pion track. No particle identification (P.I.D.) is required. The final tracking and P.I.D. acceptance for the fully reconstructed final state $D^* \to D^0\pi^+$, $D^0 \to K^+K^-$ is 11%. The primary vertex is reconstructed with great efficiency independent of the D^0 vertex, due to the relatively large multiplicity in these events (on average, the multiplicity in this reconstructed primary vertex is about 12). The last cut applied in this simple analysis is the usual detachment between the primary and secondary vertices, L/σ_L. The distribution of this quantity for the generated $D^0 \to K^+K^-$ decay vertices is shown in Fig. 11.28, and gives us a final acceptance of 4.8%, 3.0%, 1.1% and 0.2% cutting at $L/\sigma_L > 3$, 5, 10 and 20 respectively.

We assume that the dominant background comes from charm. The K^+K^- mass plot corresponding to 100,000 generated charm events is shown in Fig. 11.29, cutting at moderate values of L/σ_L. The observed signal to noise is acceptable at this stage, and should improve after imposing the following vertex cuts:

- A tighter χ^2 cut on the secondary vertex
- A "point back" cut, requiring that the D^0 track points back to the primary vertex, or conversely, that the distance of closest approach (DCA) to this primary vertex vanishes within measurement errors.
- The K^- and K^+ tracks should not point back to the primary.
- Isolation cut: Since the D^0 decay we are attempting to detect is fully reconstructed, no other tracks should have a small DCA with respect to this D^0 vertex.
- If another secondary vertex is found, make sure that K^+K^- tracks forming the D^0 vertex do not point back to that secondary vertex.

[1] A Charm photoproduction experiment which ran at Fermilab, 1987-1991

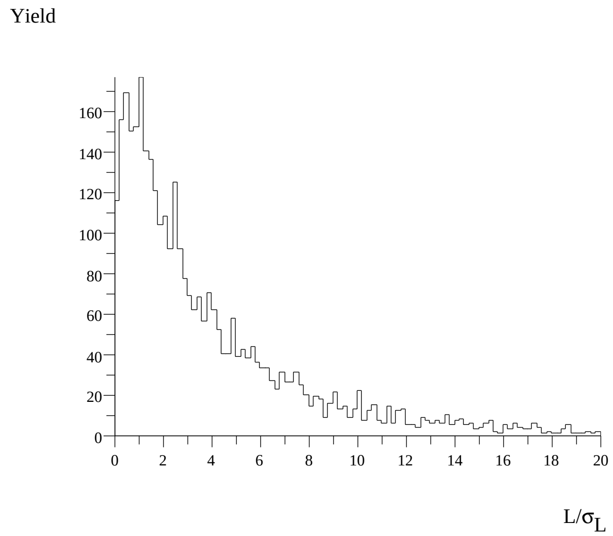

Figure 11.28: The L/σ_L distribution for the generated $D^0 \to K^+K^-$

All these cuts have been used in one form or another by various fixed target experiments for this decay mode and many others.

An effective acceptance of 0.2% could be obtained with acceptable signal to noise. This includes a trigger efficiency of 10% (we hope to increase the trigger efficiency to this level with optimization for charm). Assuming a total charm D* cross section of 1 mb, BTeV will produce and detect about 10 million such decays in 10^7 seconds running at a luminosity of $2 \times 10^{32}\mathrm{cm}^{-2}\mathrm{s}^{-1}$. In principle, this will give us a statistical error of roughly 3×10^{-4} on a D^{*+} / D^{*-} asymmetry assuming no background. We hope to achieve sensitivities below 1×10^{-3} even when backgrounds are present.

We believe a similar level of sensitivity is possible in searches for direct CP violation in D^+ decays as well. Although there is no D^* tag to reduce backgrounds, the longer lifetime of the D^+ allows harder L/σ_L cuts, and you get back the efficiency lost by requiring the bachelor pion to be found.

A proposed improvement in statistical accuracy of 1×10^{-4} is meaningless if systematic errors are not seriously taken into account. In photoproduction, the systematic errors were as big as the statistical ones, and were primarily due to uncertainties in estimating the effective acceptance versus true lifetime and to background subtraction. Such uncertainties originate in poorly defined primary vertices, a problem we hope to resolve in a collider environment where the clean track multiplicity is higher. In photoproduction a dominant source of background is secondary interactions in the target, which is not a problem at the collider.

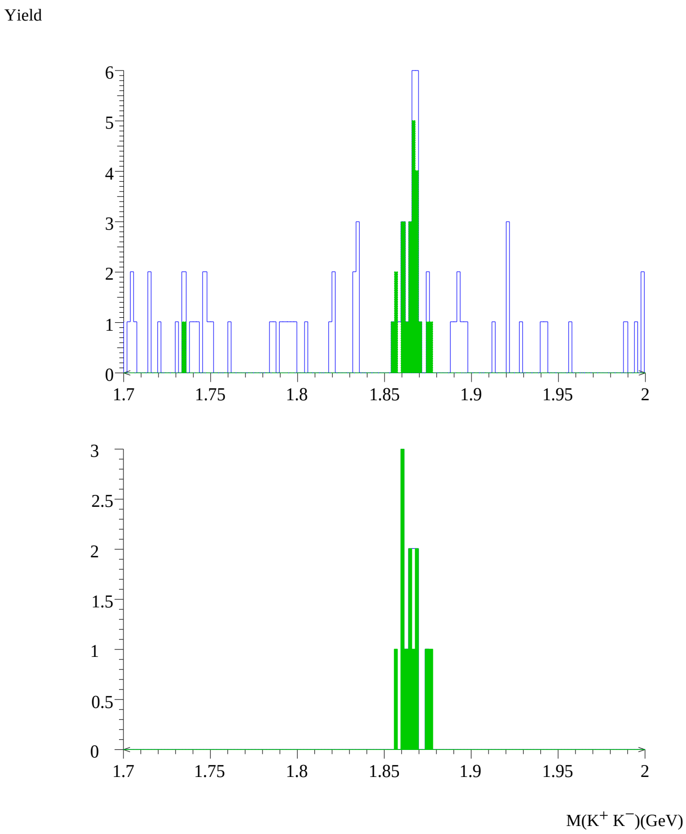

Figure 11.29: The K^+K^- invariant mass distribution from 100,000 generic Charm events, where the filled histogram contains the signal $D^* \to D^0\pi$, $D^0 \to K^+K^-$ (charge conjugation implied), while the open histogram contains all recorded events in the sample. A $|M(D^*) - M(D^0) - 0.1456| < 2$ MeV cut is imposed. In the top (bottom) plot a requirement of $L/\sigma_L > 0$ ($L/\sigma_L > 3$) is made.

11.10 Charm physics with a wire target

We anticipate that we will be able to run with a wire target before we are able to run in collider mode at C0. This will allow us to take data for charm physics at an earlier date, before the full BTeV detector is ready to install. The charm physics program with the full BTeV detector is discussed in Section 11.9; here we discuss the physics potential of the partially instrumented detector. We consider a thin target in the halo of the proton beam and a vertex detector of some combination of pixel and microstrip planes, covering the same downstream geometrical acceptance as the final detector. Although the full BTeV trigger may not be available at this time, we discuss a possible trigger for this mode of running.

11.10.0.1 Target and interaction rate

As discussed by Marriner [24], a thin target in the beam halo will intercept beam particles that have large horizontal betatron amplitudes. Such particles will pass through the target a number of times, suffering multiple coulomb scattering until they either have a nuclear interaction in the target, or are scattered so far that they are intercepted at an aperture limit of the accelerator. This analysis suggests it is advantageous to have a low-Z material for the target, *e.g.* beryllium or carbon. The interaction rate is then determined not by the thickness of the target, but by the rate at which particles leave the circulating beam. Marriner estimates an interaction rate on the order of $10^5\,\mathrm{s}^{-1}$. This is likely to be a lower limit, which could be increased by a factor of 10 or more if low β is available in C0 at the start of Run II. We propose further study of these considerations jointly with the Beams Division.

11.10.1 Vertex detector and trigger

An advantage of fixed-target mode is that the z-coordinate of the primary interaction is localized to the target. Thus the vertex detector only needs to cover about half the length that it needs in collider mode. The steps of the trigger which find where the interaction took place are also simplified. The algorithms of the full trigger can be tested on a reduced inventory of processors.

We have been studying a simplified trigger based on p_t of the tracks for use in this part of the charm program. It has been established that this is a powerful signal for charm in fixed-target interactions [25], and this is confirmed in our simulations using Pythia and MCFast. It has the following advantages in the early stages of the evolution of the detector and trigger:

- The overall interaction rate may initially be lower than in collider mode, so the requirements on performance of the trigger are reduced, since a more modest rejection is acceptable at Level I.

- Charm hadron mean lifetimes are shorter than B hadrons, so a p_t trigger will be more efficient than a vertex trigger.

- $D^* \to D\pi$ can be isolated without strong vertexing cuts offline, so it is advantageous not to impose these at the trigger stage.
- Tests of vertexing software can be made on relatively unbiased samples.

We have studied two versions of a p_t trigger: (1) using the track with the highest $|p_t|$ in the event, and (2) using the sum of $|p_t|$ for all reconstructed charged tracks. Each of these can give some rejection of background, but a combination of the two measurements can give an enhanced rejection. For example, a trigger efficiency of 60% for charm can be achieved with a rejection on the order of 10, as shown in figure 11.30.

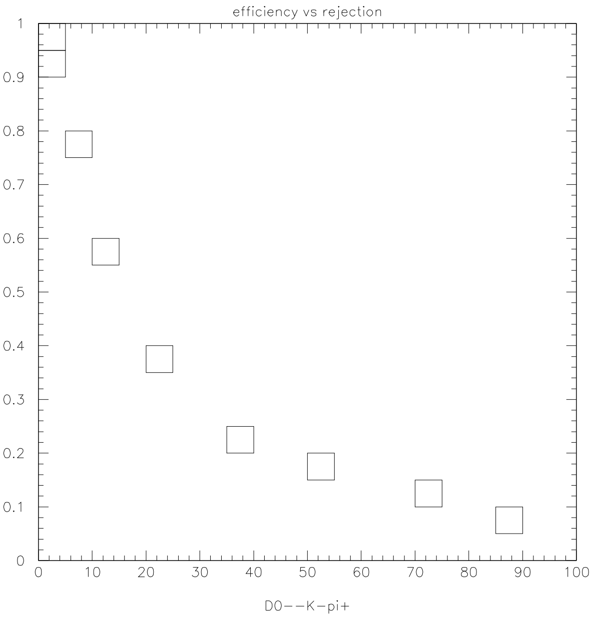

Figure 11.30: Trigger efficiency for $D^0 \to K^-\pi^+$ vs non-charm background rejection factor.

11.10.2 Reconstruction

Work is continuing on the definition of appropriate analysis cuts and the likely reconstruction efficiency for triggered events: preliminary results suggest this will be on the order of 20% for the more abundant modes. We compare this with the experience of E791, where similar values were achieved.

11.10.3 Physics reach

As an example of the potential of this mode of running, we present an estimate of the annual yield of $D^0 \to K^-\pi^+$ events which could be achieved (Table 11.12).

Table 11.12: BTeV/C0 Summary of parameters for wire target running

Property	Value	Comment
Interaction rate	$10^5 - 10^6\,\mathrm{s}^{-1}$	thin C target
Charm cross-section	25μb/nucleon	2×10^{-3} of total for $A = 12$
Charm rate	$200 - 2000\,\mathrm{s}^{-1}$	
Geometrical acceptances:		
$D^0 \to K^-\pi^+$	74%	loss mostly in beam gap
$D^{*+} \to D^0\pi^+ \to K^-\pi^+\pi^+$	61%	
Fraction of total charm which produces accepted $D^0 \to K^-\pi^+$	3.5%	including $\overline{D^0} \to K^+\pi^-$
Trigger efficiency for $D^0 \to K^-\pi^+$	60%	for accepted events
Background rejection	$\times 10$	
Level I trigger rate	$10^4 - 10^5\,\mathrm{s}^{-1}$	
Number of triggered $D^0 \to K^-\pi^+$ events	$3 - 30\,\mathrm{s}^{-1}$	
Offline reconstruction efficiency	20%	
Estimated number of reconstructed $D^0 \to K^-\pi^+$	$10^7 - 10^8$	per 10^7 sec

Bibliography

[1] "Determining the CP-violating phase γ",R. Aleksan, I. Dunietz, B. Kayser, Z. Phys C **54**, 653-659 (1992); R. Aleksan, B. Kayser and D. London, "In Pursuit of γ," DAPNIA/SPP 93-23, hep-ph/9312338.

[2] "Determination of the CP-violating phase γ by a sum over common decay modes to B_s and $\overline{B}_s$ ",R. Aleksan, A. Le Yaouanc, L. Oliver, O. Pene, J.-C. Raynal, Z. Phys C **67**, 251-260 (1995).

[3] D. Atwood, I. Dunietz and A. Soni, PRL 78, 3257(1997).

[4] M. Gronau and D. Wyler, *Phys. Lett.* B **265**, 172 (1991).

[5] M. Gronau and J. Rosner, CALT-68-2142, hep-ph/9711246 (November 1997).

[6] R. Fleischer and T. Mannel, hep-ph/9704423.

[7] R. Godang *et al*, *Phys. Rev. Lett.* **80**, 3456 (1998).

[8] A. Falk, A. Kagan, Y. Nir and A. Petrov, JHU-TIPAC-97018 (December 1997).

[9] BTev EOI (May 1997).

[10] "J/ψ and $\psi(2S)$ Production in $p\overline{p}$ Collisions at $\sqrt{s} = 1.8TeV$", CDF Collaboration, FERMILAB-PUB-97/024-E

[11] " The CDF II Detector Technical Design Report", CDF collaboration, FERMILAB-Pub-96/390-E

[12] http://www-pat.fnal.gov/mcfast/version_doc/v2_6_2/mcfast/mcfast_advanced.html

[13] O.R. Long, *et al.*, "Monte Carlo Simulation of $B_d^0 \to \pi^+\pi^-$ from pp Interactions at $\sqrt{s} = 40$ TeV", UPR/216E, PRINCETON/HEP/92-07, SSCL/PP/139 (1992).

[14] F. Abe et al., The CDF Collaboration, Phys. Rev. **D54**, 6596 (1996). FERMILAB-PUB-96/119-E.

[15] *The BaBar Physics Book*, edited by P. Harrison and H. Quinn, SLAC-R-504, January 1999.

[16] " The CDF II Detector Technical Design Report", CDF collaboration, FERMILAB-Pub-96/390-E (1996).

[17] A. Ali, "Rare B Decays in the Standard Model", *Beauty '96*, North Holland Press, 1996, the Netherlands, Table 1, page 13 and references therein.

[18] QQ is developed and maintained by the CLEO Collaboration. See http://www.lns.cornell.edu/public/CLEO/soft/QQ/ For the studies reported here, it is used for its model of the decays of hadrons containing heavy flavors.

[19] P. McBride and S. Stone, Nucl.Instrum.Meth. **A**368(1995) 38-40.

[20] R. Kutschke, BTeV Internal Note, 97/9, June 1997.

[21] K.T. McDonald, "Maximum Likelihood Analysis of CP Violating Asymmetries", PRINCETON-HEP-92-04, Sep 1992. 12pp, unpublished.

[22] K. Sterner and W. Selove, Univ. of Pa. Report UPR-237E, May 1997.)

[23] P.L. Frabetti *et al.*, *Nucl. Instrum. Methods.* **A 320**, 519 (1992).

[24] J.Marriner, "Operation of the C0 experimental region with a fixed (internal) target", April 1997, unpublished.

[25] D.C.Christian, "Triggers for a high-sensitivity charm experiment", in proceedings of CHARM2000 workshop, Fermilab-conf-94/190 (1994).

Chapter 12

Comparison of BTeV to Other Experiments

12.1 Comparison with CDF, D0, CMS, and ATLAS

Both CDF and D0 have measured the b production cross section [1]. CDF has contributed to our knowledge of b decay mostly by its measurements of the lifetime of b-flavored hadrons [2], which are competitive with those of LEP [3] and recently through its discovery of the B_c meson [4]. CDF has also seen the first hint for CP violation in the b system [5]. These detectors were designed for physics discoveries at large transverse momentum. It is remarkable that they have been able to accomplish so much in b physics. They have shown that it is possible to do b physics in the environment of a hadron collider.

However, these detectors, and the new central detectors ATLAS and CMS are very far from optimal for b physics. BTeV has been designed with b physics as its primary goal. To have an efficient trigger based on separation of b decays from the primary, BTeV uses the large η region where the b's are boosted. The detached vertex trigger allows collection of interesting purely hadronic final states such as $\pi^+\pi^-$, $\rho\pi$, $D_s^+\pi^-$ and $D_s^+K^-$. It also allows us to collect enough charm to investigate mixing and CP violation.

The use of the forward geometry also allows for excellent charged hadron identification with a gaseous RICH detector. This is crucial for many physics issues such as separating $K\pi$ from $\pi\pi$, $D_s\pi$ from D_sK, kaon flavor tagging, etc..

Furthermore an experiment that plans on answering all the open questions in b physics, requires a high quality electromagnetic calorimeter. Installation of such a calorimeter in the CLEO detector made new physics vistas possible and such a device in BTeV allows for the measurement of several crucial physics final states such as $B^o \to \rho\pi$, and $B_s \to J/\psi\eta'$. The only central detector that is planning to have a high quality electromagnetic calorimeter is CMS.

Finally, BTeV has all the crucial elements required to study any newly suggested b or charm processes or uncover new physics. The crucial elements are:

- a detached vertex trigger in the first trigger level,

- highly efficient particle identification across the entire momentum range with good ($\approx$ 100:1) background rejection,
- an electromagnetic calorimeter with sufficiently good energy resolution and efficiency to fully reconstruct rare B decay final states with single photons or neutral pions.

12.2 Comparison with e^+e^- B Factories

Most of what is known about b decays has been learned at e^+e^- machines [6]. Machines operating at the $\Upsilon(4S)$ found the first fully reconstructed B mesons (CLEO), B^o-$\overline{B}^o$ mixing (ARGUS), the first signal for the $b \to u$ transition (CLEO), and Penguin decays (CLEO). Lifetimes of b hadrons were first measured by experiments at PEP, slightly later at PETRA, and extended and improved by LEP [6].

The success of the $\Upsilon(4S)$ machines has led to the construction at KEK and SLAC of two new $\Upsilon(4S)$ machines with luminosity goals in excess of $3 \times 10^{33}\mathrm{cm}^{-2}\mathrm{s}^{-1}$. These machines will have asymmetric beam energies so they can measure time dependent CP violation. They will join an upgraded CESR machine at Cornell that has symmetric beam energies. These machines will investigate only B^o and $B^{\pm}$ decays. They will not investigate B_s, B_c or Λ_b decays.

Table 12.1 shows a comparison between BTeV and an asymmetric e^+e^- machine for measuring the CP violating asymmetry in the decay mode $B^o \to \pi^+\pi^-$. In Table 12.2 we show a similar comparison for the final state $B^- \to \overline{D}^o K^-$, a mode that could be used to determine the CKM angle γ. It is clear that the large hadronic b production cross section can overwhelm the much smaller e^+e^- rate. Furthermore, the e^+e^- B factories do not have access to the important CP violation measurements that need to be made in B_s decays.

Table 12.1: Number of tagged $B^o \to \pi^+\pi^-$ ($\mathcal{B}$=0.75×10^{-5})

	$\mathcal{L}(\mathrm{cm}^{-2}\mathrm{s}^{-1})$	σ	# $B^o/10^7$s	signal efficiency	tagging ϵD^2	# tagged
e^+e^-	3×10^{33}	1 nb	3.0×10^7	0.4	0.4	46
BTeV	2×10^{32}	100μb	1.4×10^{11}	0.03	0.1	3400

12.3 Comparison with LHC-B

LHC-B is an experiment proposed for the LHC with almost the same physics goals as BTeV [7]. Here we address the issue of how BTeV can compete with LHC-B. LHC-B is being designed to run at a luminosity of 2×10^{32} $\mathrm{cm}^{-2}\mathrm{s}^{-1}$, the same as BTeV's goal. There are

Table 12.2: Number of $B^- \to \overline{D}^o K^-$ ($\mathcal{B}$=1.5 × 10^{-7})

	$\mathcal{L}$(cm^{-2}s^{-1})	σ	# $B^-/10^7$s	signal efficiency	# of events
e^+e^-	3×10^{33}	1 nb	3.0×10^7	0.5	2
BTeV	2×10^{32}	100μb	1.4×10^{11}	0.015	320

several inherent advantages and disadvantages that LHC-B has compared with BTeV. The issues that favor LHC-B are:

- The b production cross-section is expected to be about five times larger at the LHC than at the Tevatron, while the total cross-section is only 1.6 times as large.
- The mean number of interactions per bunch is expected to be about 3 times lower at the LHC than at the Tevatron (at 132 ns bunch spacing).

The issues that favor BTeV are:

- BTeV is a two-arm spectrometer, which increases the signal by a factor of two compared with LHC-b.
- The short bunch spacing at the LHC, 25 ns, makes first level detached vertex triggering more difficult than at the Tevatron. It is difficult for the vertex detector electronics in LHC-b to settle in 25 ns, while BTeV has a more relaxed 132 ns. In fact, the current plan of LHC-b is to trigger in their first trigger level on muons, electrons or hadrons of moderate p_t, and detect detached vertices in the next trigger level.
- The seven times larger beam energy at the LHC makes the range of track momenta that need to be momentum analyzed and identified much larger and therefore more difficult. The larger energy also causes a large increase in track multiplicity per event, which makes pattern recognition and triggering more difficult.
- The interaction region at the Tevatron is three to six times longer along the beam direction than at LHC (σ_z = 5 cm), which allows BTeV to able to accept events with two or even three interactions per crossing, since the interactions are well separated. LHC-b currently vetos crossings with more than one interaction.
- BTeV is designed to have the vertex detector in the magnetic field thus allowing the rejection of low momentum tracks at the trigger level. Low momentum tracks have large multiple scattering which can cause false detached vertices leading to poor background rejection in the trigger.

- BTeV is designed with a high quality $PbWO_4$ electromagnetic calorimeter, that provides high resolution and acceptance for interesting final states with γ's, π^o's, and $\eta^{(\prime)}$'s.
- Use of a detached vertex trigger at Level 1 allows for an extensive charm physics program absent in LHC-b. It also allows for a more uniform collection of b triggers.

We have more than compensated for LHC-b's initial advantages in b cross-section due their higher center-of-mass energy. In fact, the high energy actually works in many ways as a disadvantage. For example, LHC-b needs two RICH counters to cover the momentum range in their one arm. Particle identification and other considerations force LHC-b to be longer than BTeV. Its single arm is as long as both BTeV arms put together. This causes the transverse size of LHC-b to be four times that of each arm of BTeV, and this allows them only to cover the same solid angle as one of BTeV's two arms. It is expensive to instrument all of this real estate with high qualtiy particle detectors. Thus, the total cost for LHC-b based only on instrumented area, (a naive assumption) would be twice the total cost for BTeV, even though LHC-b would cover only half the solid angle.

Bibliography

[1] K. Abe *et al*, (CDF), *Phys. Rev. Lett.* **75**, 1451 (1995); S. Abachi *et al*, (D0), *Phys. Rev. Lett.* **74**, 3548 (1995). See also the UA1 measurement C. Albajar *et al*, *Phys. Lett.* B**186**, 237 (1987); B**213**, 405 (1988); B**256**, 121 (1991).

[2] K. Abe *et al*, (CDF), *Phys. Rev. Lett.* **76**, 4462 (1996); ibid **77**, 1945 (1996); K. Abe *et al*, (CDF), *Phys. Rev. D* **57**, 5382 (1998).

[3] T. Junk, "A Review of B Hadron Lifetime Measurements from LEP, the Tevatron and SLC," in Proceedings of the 2nd Int. Conf. on *B Physics and CP Violation*, Univ. of Hawaii, (1997), ed. T. E. Browder *et al*, World Scientific, Singapore (1998).

[4] K. Abe *et al*, (CDF), "Observation of B_c Mesons in $p-\overline{p}$ Collisions at $\sqrt{s} = 1.8$ TeV," hep-ex/9804014 (1998).

[5] M. Paulini, "B Lifetimes, Mixing and CP Violation at CDF," Review article to appear in the Int. Journal of Modern Physics A, hep-ex/9903002 (1999).

[6] See *B Decays, revised 2nd Edition* ed. S. Stone, World Scientific, Singapore, (1994).

[7] "LHCb Technical Proposal," CERN/LHCC 98-4, LHCC/P4 (1998).